

# Emission Line Galaxies in the STIS Parallel Survey I: Observations and Data Analysis<sup>1</sup>

Harry I. Teplitz,<sup>2,3</sup> Nicholas R. Collins,<sup>4</sup> Jonathan P. Gardner, Robert S. Hill,<sup>4</sup> Sara R. Heap, Don J. Lindler,<sup>5</sup> Jason Rhodes,<sup>6</sup> & Bruce E. Woodgate

*Laboratory for Astronomy and Solar Physics, Code 681, Goddard Space Flight Center,  
Greenbelt MD 20771*

*Electronic mail: hit@ipac.caltech.edu*

## ABSTRACT

In the first three years of operation STIS obtained slitless spectra of  $\sim 2500$  fields in parallel to prime HST observations as part of the STIS Parallel Survey (SPS). The archive contains  $\sim 300$  fields at high galactic latitude ( $|b| > 30$ ) with spectroscopic exposure times greater than 3000 seconds. This sample contains 220 fields (excluding special regions and requiring a consistent grating angle) observed between 6 June 1997 and 21 September 2000, with a total survey area of  $\sim 160$  square arcminutes. At this depth, the SPS detects an average of one emission line galaxy per three fields. We present the analysis of these data, and the identification of 131 low to intermediate redshift galaxies detected by optical emission lines. The sample contains 78 objects with emission lines that we infer to be redshifted [OII]3727 emission at  $0.43 < z < 1.7$ . The comoving number density of these objects is comparable to that of H $\alpha$ -emitting galaxies in the NICMOS parallel observations. One quasar and three probable Seyfert galaxies are detected. Many of the emission-line objects show morphologies suggestive of mergers or interactions. The reduced data are available upon request from the authors.

---

<sup>1</sup>Based on observations made with the NASA/ESA *Hubble Space Telescope*, obtained from the data archive at the Space Telescope Science Institute, which is operated by the Association of Universities for Research in Astronomy, Inc., under NASA contract NAS 5-26555.

<sup>2</sup>Catholic University of America, Research Associate

<sup>3</sup>New affiliation – SIRTf Science Center

<sup>4</sup>SSAI

<sup>5</sup>Sigma Space Corporation

<sup>6</sup>NRC Fellow

*Subject headings:* cosmology: observations — galaxies: evolution — galaxies: fundamental parameters —

## 1. Introduction

The relative pointing of instruments on the Hubble Space Telescope allows for parallel observation during targeted science exposures. Parallel fields are essentially random pointings on the sky, being separated by 5-8 arcminutes from the prime target. Extensive imaging of parallel fields was possible with WFPC2, and the Medium Deep Survey obtained hundreds of fields (c.f. Griffiths et al. 1994). With the addition of the slitless spectroscopic capabilities of STIS (Kimble et al. 1998) and NICMOS (Thompson et al. 1998), parallel observations now allow HST to conduct redshift surveys in large numbers of random fields without negatively impacting the duty cycle of the telescope (see Gardner et al. 1998, McCarthy et al. 1999, Yan et al. 1999). These untargted redshift surveys explore a new regime in galaxy evolution, as they are less subject to a bias induced by cosmic variance than pencil beam surveys (e.g. Cohen et al. 2000) and detect fainter objects than wide field surveys (e.g. CFRS; Hammer et al. 1997). The slitless spectroscopy requires comparable deep imaging for object identification; thus the redshift survey is accompanied by high resolution imaging.

In this paper, we present the analysis of the deepest spectroscopic fields in the STIS parallel survey (SPS). STIS parallel spectra were taken over the 5300-10000 Å range during the course of the program. We have searched for emission line galaxies, in particular [OII]-emitting galaxies at redshift  $0.43 < z < 1.7$ . Our motivation is to determine the comoving density of star-formation at these redshifts as inferred from [OII] emission (Teplitz et al. 2002; hereafter Paper II). We will discuss the target selection in section 2, the data reduction, line identification and measurement in section 3, and the results in sections 4 and 5.

## 2. Target Selection

The SPS data were obtained in pairs of spectroscopic exposures and direct images of each field. The spectroscopic (dispersed) exposures were taken with the G750L low resolution grating, which has a dispersion of 4.92 Å per pixel and a point source resolving power of  $\sim 750$  at 7500 Å. The resolving power decreases for extended objects in slitless spectroscopy, as the resolution element is convolved with the galaxy profile. The spectra cover the range of approximately 5300-10000 Å, depending on object position within the field. The sensitivity falls off sharply at the blue end and gradually at the red end. We can detect [OII] at

$0.43 < z < 1.68$ , [OIII]5007 at  $z < 1$ , and H $\alpha$  at  $z < 0.52$ . The spectroscopic exposures are binned by a factor of two in the spatial dimension in order to improve read noise. The SPS includes G750L observations with the grating angle set to provide different center wavelengths. To ensure as uniform a dataset as possible, we limit our dataset to spectra with a center wavelength of 7751Å. Direct imaging data are taken without a filter, providing photometry integrated over CCD-response limited wavelength range ( $\sim 2200 - 11000$  Å, see Baum et al. 1996), referred to as 50CCD magnitudes.

During the period 6 June 1997 and 21 September 2000, STIS observed  $\sim 2500$  parallel fields. Our goal is to study optical emission lines at intermediate redshift, so our targets will be faint, and we select only the deepest exposures. Through trial and error we determined that 3000 seconds were needed to reliably detect emission line objects in random fields. We also require a deep image (300 seconds) to establish the wavelength scale, properly identify the objects, and measure their photometric characteristics.

STIS parallel fields lie 5 to 8 arcminutes from the targeted position, depending on which instrument is prime. Only those fields that are not contaminated by the prime science target are usable for this study. Thus targets near the galactic plane ( $|b| < 30$ ), nearby galaxies, or galaxy clusters are excluded.

The data were taken under a variety of observing plans. In some cases all imaging (or spectroscopic) exposures had the same integration time, in other cases the integration times were optimized to fill the orbit. The cosmic ray (CR) rejection algorithm is more effective in cases of equal integration time, and this should be considered in planning of future surveys. In a few fields the automated CR-rejection algorithm failed to produce acceptable results, and we discard those fields from the survey.

After rejecting contaminated fields, 219 SPS fields meet our requirements. The sample contains fields with more than 30,000 seconds of integration time, but the distribution is strongly weighted towards the shortest allowed exposure time (3000 seconds; see Figure 2).

Dithering of the observation was determined by the prime instrument. Typically this provided a few tens of pixels in both the  $x$  and  $y$  directions. The regions on the edges with poor overlap are not included in the survey. Similarly, a bright star or local galaxy can obscure significant area of the background sky. These obscured regions are not included in the survey area. Table 1 lists the exposure time for both imaging and spectroscopic exposures for each field, together with the pointing information and limiting flux (see below), and the areal coverage of the good region.

We searched the NASA/IPAC Extragalactic Database (NED) for known objects in each field. Three fields contain objects with previously reported redshifts, and many fields contain

previously reported objects without certain redshifts. NED objects are described in Table 2.

### 3. Data Reduction

The first step in the data reduction was identification of fields with common pointing. Observations were considered as co-pointed if they were centered within  $5''$  of each other, and they were processed as a group. Each exposure was processed through the basic data reduction software, CALSTIS. This software was developed by the STIS Investigation Definition Team (IDT), and it is similar to the IRAF version available from STScI. Briefly, the data were bias and dark subtracted, flat fielded, and bad pixels were repaired. The bias subtraction included an overscan fit to account for small temporal variations. Since the 2D spectroscopic exposures are binned by a factor of two in  $y$ , the dark was binned in software before subtraction. We do not find that this binning introduces any artifacts, but it is a step that must be checked carefully when applied. The flat fielding was performed in two steps: first, a pixel-to-pixel flat was applied, and then a correction was made for low frequency variation across the CCD induced by vignetting. The flat fields are monochromatic and so do not correct for fringing at long wavelengths in the spectra. Fringing can cause increased noise in the measurement of line fluxes at the  $\sim 10\%$  level. The bad pixel repair was based on the best available (i.e., taken closest in time) bad pixel mask from the archive. Each bad pixel was replaced by the average of its neighbors, and that pixel was flagged in the error array. For direct images the eight nearest pixels were used, but for dispersed images only the left and right neighbors were averaged in order to use data in the same spectrum. A second bad pixel correction was also performed on the output from CALSTIS in order to “preclean” the data before CR rejection. This second correction checked for single, isolated pixels with outlying data values.

After the “calstis” reduction, the offsets between dithered exposures were calculated. The offsets were determined by cross-correlation of source positions in each image. Spectroscopic exposures were assumed to have the same offset as the image taken in the pair. In some cases, however, there were spectroscopic exposures that were taken without a direct image at the exact position, and the shift needed to be determined from the astrometry in the FITS header. In these cases the shifts are good to about a pixel, but are not as accurate as the subpixel shifts determined from the extracted sources. In order to measure source positions in each image, a crude CR rejection must be performed. The algorithm looks for groups of high count-rate pixels that are too compact or too highly peaked to be real objects. Since it is not necessary to preserve all real sources at this step, the precleaning parameters are set to make the rejection severe. Sources were identified using the SExtractor software

(Bertin & Arnouts 1996).

Once offsets had been determined, individual exposures were registered, with bilinear interpolation for subpixel shifts. Cosmic rays in the images were identified in background subtracted copies of the images. The background was determined in the direct images using two dimensional smoothing after source removal. This procedure is modelled on the SExtractor background subtraction. For the spectroscopic images, a one dimensional column-by-column median was used for background subtraction. The stack of registered images was cleaned by omitting outliers in the distribution of pixel values separately at each pixel position. The cleaned images were combined into a final frame using the mean of pixels remaining at each position. The reduced data were normalized to counts per second per unbinned pixel.

### 3.1. Identifying, Extracting, and Measuring Emission Lines

Each reduced spectroscopic frame was searched by eye for emission lines. Three of us (HIT, NRC, JR) examined every field. Lines were only considered real if there was unanimous agreement (though independent discovery of each line was not required). Figure 1 shows an imaging/slitless spectrum pair, with strong emission lines. In many frames, bad pixels are present that must be examined carefully by hand to distinguish them from real emission lines. At a minimum, a real line is required to have significant flux in multiple pixels. We set a significance threshold of  $\sigma = 2.5$  for the strongest emission line in an object in order for it to be considered. Further, we do not consider any possible emission lines that cannot be associated with an object in the direct image. We detect emission lines in 134 objects. Objects at low redshift ( $z < 0.2$ ) are well resolved and the emission lines often appear to originate in small knots; in those cases we did not measure the line flux, but we will present the object identification and redshift.

For extraction, the position of the spectrum in the 2D frame must be known relative to the source position in the image. The dispersed frames have a small anamorphic magnification (less than 2%), which is included in the extraction. Contemporaneous wavelength calibrations cannot be taken for each individual parallel observation. The wavelength scale is determined from an empirical fit to on-orbit data taken early in the project. This scale appears to be stable at the  $\sim 1 - 2$  pixel level, with variations arising from mechanism non-repeatability and thermal motion. The wavelength scale for an extracted spectrum with pixels,  $x_i$  is

$$\lambda_i = \frac{x_i - c_0 - c_1 P_x}{d_0 + d_1 P_y} + \lambda_c \quad (1)$$

where  $(P_x, P_y)$  are the pixel position of the galaxy center in the direct image, and the value of the constants depends on the grating settings. For the SPS,  $c_0 = 4.50$ ,  $c_1 = 0.99031$ ,  $d_0 = 0.204737$ ,  $d_1 = 4.468 \times 10^{-7}$ , and  $\lambda_c = 7764.58 \text{ \AA}$ . We use a linear wavelength scale, as the quadratic terms in the solution would be at the subpixel level. The value of  $(P_x, P_y)$  are accurate on the integer pixel level. Combined with the repeatability of the scale, wavelength calibration uncertainty is  $\sim 2 - 3$  pixels. Emission line wavelengths are measured to within 1 pixel, so the total redshift uncertainty is on the order of 3 pixels ( $\sigma_z \sim 0.004$  for [OII] at  $z = 0.9$ ).

Spectra were extracted by simple summation along the columns covered by the wavelength range. The width of the extraction box was set by hand for each object. A small ( $\lesssim 15\%$ ) "slit correction" was applied to the extraction based on the width of the box, compared to the profile of the object. Spectra were sky-subtracted based on two sky windows, one on either side of the spectrum. The width of these windows, and their offset from the spectrum, were adjusted manually for extraction, to achieve minimal contamination from other objects in the field. For each column in the spectrum, the average pixel value in that column in each sky window is measured, and a line is fit to the two points, giving a sky value at each pixel in the spectrum. Before subtracting, these interpolated sky values are smoothed row by row, using a median filter followed by two iterations of a mean filter. The extracted spectra were divided by the sensitivity function to convert from DN/s/pixel to flux units.

Lines were measured in extracted spectra by interactively fitting a gaussian to the line profile and integrating. Continuum measurements were made in the spectra themselves in regions near the line. For several bright objects the flux calibrated continuum measurements were checked against the continuum value inferred from the clear aperture photometry. There is a trade off between the poor signal-to-noise in the spectroscopic continuum, and the uncertainty in the slope of the continuum needed to use the aperture photometry to infer the continuum. For consistency, the equivalent width (EW) of each line was calculated from the local continuum measurement rather than the photometric value. This procedure leads to poor EW measurements in the faintest, high EW objects. However, for the scientific analysis, we will need to know the EW value with the greatest certainty for objects with low EW values, and thus objects with better continuum measurements (see Paper II).

### 3.2. Single Line Objects

We detect only single lines in 94 of the 131 objects. In order to assign a rest wavelength to single-line objects, it is necessary to appeal to common sense constraints. We assume

that any lone emission line is either  $H\alpha$  or the next strongest optical line associated with star-formation, [OII]3727 (Kennicutt 1998).  $Ly\alpha$  emission at  $z > 5$  is not considered a possibility, as there is often some flux detected blueward of the line, and in most cases the objects are relatively bright.

The [OIII] doublet at 4959, 5007 Å is also sometimes strong in star-forming galaxies. The ratio of the double is 1:3.1, so it is possible that a low signal to noise detection of a single line could be 5007 (which would also imply weak  $H\beta$  emission at 4861Å). Typically, at low redshift [OIII] is undetected in galaxies with  $EW(H\alpha) < 40$  Å, but can be 30% the strength of  $H\alpha$  in the most vigorously star-forming objects (Kennicutt 1992). In low metallicity galaxies and HII regions, [OIII] can be as strong as  $H\alpha$  or even stronger in some cases (Terlevich et al. 1991; Izotov, Thuan, & Lipovetsky 1994). At high redshift ( $z > 2.5$ ), [OIII] has also been detected galaxies with a line strength comparable to  $H\alpha$  in lower metallicity ( $1/3 Z_{\odot}$ ) galaxies (Pettini et al. 2001; Teplitz et al. 2000).

However, in our spectra [OIII]5007 is not the most likely identification for a single line. At  $z < 0.5$ , H-alpha would still be in the nominally observable wavelength range, and at higher redshifts [OII] would be in the range at the blue end, and in some cases [OII] can be 50-200% the strength of [OIII] (e.g. Kobulnicky, Kennicutt, & Pizagno 1999). In addition, for the  $\sim 10$  single line objects with good ( $\sigma > 5$ ) detections, one might expect to see some evidence of either [OIII]4959 or  $H\beta$  if the line were [OIII]5007.

We do not necessarily expect to see [NII] emission from the  $H\alpha$  emitters, as [NII] can be 0.1 to 0.3 the strength of  $H\alpha$ . Also, at low redshift [NII] may be hard to resolve from  $H\alpha$ , given that spectra lose resolution for larger objects.

Given only the choice of [OII] and  $H\alpha$ , any line at wavelengths shortward of 6563 Å must be [OII]. Similarly an emission line that would place an  $H\alpha$ -emitter at a low redshift ( $z < 0.2$ ) might be expected to appear noticeably large and bright in the image. We make this assumption, and thus do not consider the possibility that the survey might detect extremely low mass galaxies at low redshift.

The ratio of  $H\alpha$  to [OIII]5007 emission is typically 2-3 to 1 (Kennicutt 1992) and the ratio of  $H\alpha$  to  $H\beta$  is 2.86 to one. Thus a single line at the red end of the spectrum is taken to be [OII] if there is no evidence of [OIII] or  $H\beta$  where they would have been expected had the line been  $H\alpha$ .

Finally, there are 28 objects that give no indication as to the rest wavelength of the line. Since the survey covers considerably more volume for [OII] emitters, we assume that these lines are [OII]. It should be kept in mind, then, that the density of [OII] emitters inferred is an upper limit and that some downward correction (25% or less) might be expected.

The large percentage of single line objects in the sample is in part a result of the limited spectral coverage. Since objects near the edge of the field of view have their spectral range truncated, [OII]-emitters for example are very likely to be single line objects. Indeed, 40 of the 64 objects identified as single line [OII] emitters are at redshifts that place the next strong line ( $H\beta$ ) beyond the red end of the spectrum. The observed wavelength range of each spectrum is listed in Table 3.

A quality flag is assigned to the redshift of each galaxy. A value of 4 indicates that there are multiple emission lines and the redshift is secure. A value of 3 is assigned to galaxies for which there is a strong reason for the assignment; that is one of the following:

- (a) the wavelength of the single line is less than  $6563\text{\AA}$ , or
- (b) the wavelength of the single line would place a faint ( $m > 23$ ) and/or compact object at  $z < 0.2$ , or
- (c) the redshift of the object if it were an  $H\alpha$ -emitter would imply a non-detection of [OIII]5007.

A quality flag of 2 indicates that there is some potential problem with the assignment. Usually this indicates that the line is at a blue wavelength (option *b* above) but that no [OIII]5007 is detected at the red end of the spectrum. In a few cases, this non-detection is in a region of poor spectroscopic sensitivity ( $\lambda > 9000\text{\AA}$ ) and a quality flag of 1.5 is assigned to differentiate it. A non-detection of [OIII] in an [OII] emitter is possible, depending on the conditions in the galaxy. The [OII] : [OIII] ratio can vary from 0.1 to 10. These non-detections, if confirmed, would imply that these galaxies had unusual metallicities or ionization parameters. A quality flag of 1 indicates that the redshift is poor, and that it is based solely on the volume of the survey.

### 3.3. Measuring the Noise

Given a weak or virtually nonexistent continuum detection (as in many SPS spectra), it is hard to measure the signal to noise ratio of an emission line from the extracted spectrum. Instead, the noise is measured in each image and compared to the signal in the line. Since each line is a two dimensional pixel region before extraction, the noise can be measured in the sky in much the same manner as it would be for photometry in imaging. The specific method is to randomly extract a box the size of the line at thousands of positions across the frame. The

size is determined in the  $y$  direction by the width of the extraction box. In the  $x$  direction, the size is determined from the measured FWHM of the line. Each extraction includes a sky subtraction from neighboring sky windows, just as in the spectroscopic extraction. The extracted values should have a median of zero if there is no residual spatial variation in the sky. The standard deviation of the extractions is the noise in the frame for a line with that spatial and spectroscopic extent. Table 1 lists the typical  $1\sigma$  limiting fluxes for each field, based on an emission line from a galaxy with  $FWHM = 0.39''$ , and a 7 pixel wide extraction box. This size is slightly larger than the median for detected lines.

## 4. Results

We detected 131 emission line objects in the deep SPS fields. The direct image and extracted spectrum of each object are shown in figure 3-24. Each object is described in Table 3. Column (1) lists the name of the object; columns (2) and (3) give the position of the object based on the SExtractor pixel coordinates transformed to the World Coordinate System, which for HST images is good to better than  $1''$ ; column (4) gives the redshift, and column (5) the redshift quality flag; column (6) lists the photometric magnitude in the filterless direct image; columns (7)-(9) give morphological parameters measured by SExtractor; and column (10) lists the strongest lines detected in the spectrum. Line fluxes were only measured for those objects where the integrated flux for the entire galaxy could be obtained; low redshift objects with hotspot or diffuse emission were not measured, and are flagged with redshift quality flag 0. Table 4 gives the emission line measurements. Column (1) is the object name and column (2) is the measured line; columns (3)-(5) give the line flux, its signal-to-noise ratio, and the equivalent width; column (6) gives the approximate continuum signal-to-noise in one resolution element near the wavelength of the line. The continuum is measured over many resolution elements; however, the low signal-to-noise in the continuum measurements demonstrates the large uncertainty in the EW measurements.

### 4.1. Notes On Individual Objects

SPS J082344.12+292351.3 – The [OIII]4959 line may be contaminated by a bad pixel.

SPS J095240.06+435834.9 – This object shows three strong nuclei, suggesting either a triple nucleus or a projection of three edge on galaxies which appear “stacked.” Emission lines are detected only from the nucleus closest to the bottom of the image.

SPS J095628.10+694551.9 – This bright spiral shows probable  $H\alpha$  emission from knots

on the spiral arm.

SPS J100051.56+250858.6 – There are two objects in the same row that could be associated with the emission line. We assume that the line is associated with the brighter one.

SPS J103640.31-034708.1 – The blue end of the continuum (up to 6000 Å) is contaminated by a bright object in the same row.

SPS J105700.03-034400.9 – The object has a bright nucleus, perhaps indicating AGN, and a region of extended continuum suggesting a tail or jet. The continuum is contaminated by bright galaxy on the same row.

SPS J105708.69-034310.8 – There is a slight difference in inferred redshift from [OIII] and H $\alpha$ . They differ by 5Å from the prediction of the other.

SPS J105708.06-034320.1 – This object has multiple nuclei in a “train wreck” morphology.

SPS J112057.83+232306.6 – This object has a single emission line from the nucleus, although it has arm-like extensions from which no emission is seen.

SPS J115623.08+550218.1 – This spiral or irregular galaxy does not show a strong nucleus in the direct image, but has very bright knots, at least 3 of which show strong H $\alpha$  emission.

SPS J120113.92-185633.2 – This object appears to have two nuclei, perhaps indicating that it is the result of an interaction or merger, but only one of the nuclei shows strong line emission.

SPS J123102.59+121424.8 – This late-type spiral or irregular galaxy has many knots. The nucleus shows clear H $\beta$ , [OIII], and H $\alpha$  emission.

SPS J123348.78+023212.4 – The object is very diffuse; nevertheless, the line looks definite on the dispersed image.

SPS J123703.08+140803.7 – The objects appears to be the result of a merger or interaction of two objects. They are spatially separated along  $x$ .

SPS J130015.23+275336.1 – This spiral/irregular galaxy has many knots of bright continuum emission. Some of the galaxy is outside the frame. The nucleus and a few of the knots have a weak emission line, most likely H $\alpha$ .

SPS J131810.43-000453.8 – A point source with strong rest-frame UV emission lines,

identified to be a quasar at  $z=3.17$ .

SPS J132511.10+301418.3 – The continuum spectrum may be contaminated by other objects in the same row.

SPS J134429.63-000909.6 – This object is a spiral galaxy with bright knots and also faint, extended continuum. The emission line from the bar looks double in spectrum, so it maybe emitted from two hotspots, though they are hard to match up with direct image.

SPS J134608.36+015922.6 – This object shows an emission line from a double nucleus. The line appears offset in wavelength in the spectrum, because it is offset along the row. The flux measurement is the sum of the flux from both nuclei.

SPS J134721.93+021407.2 and SPS J134721.97+021405.7 – A bright galaxy and a faint companion with a double nucleus appear to be at the same redshift, though perhaps the companions are simply knots in the outer regions of the galaxy itself. The companion shows relatively stronger oxygen emission than the galaxy. Also, the spacing between the nuclei is the same as the spacing between 5007 and 4959, so that the 5007 line from the left nucleus coincides with 4959 from right nucleus; we measure 5007 from the right nucleus.

SPS J160956.65+653334.6 – This bright galaxy shows strong emission lines including [FeVII]5721 and [OI]6300, at  $z = 0.157$ . The direct image of the source is not dominated by a bright nucleus, and we infer that the object is a Seyfert.

SPS J162357.69+262830.2 – This object has strong emission lines including [FeVI], and is likely a Seyfert 1. The direct image shows a strong nucleus, but the lines appear to originate mostly in the nebulosity offset from the nucleus by 3 – 5 pixels.

SPS J162354.88+262803.5 – This bright galaxy has a previously reported redshift of  $z = 0.47473$  as a member of the galaxy cluster MS 1621.5 + 2640, which is centered at  $z = 0.4275$  near this field, by the Canadian Network for Observation Cosmology survey (CNOC; Ellingson et al. 1997). The [OII] line that was likely the basis of the CNOC redshift is clearly detected in the SPS spectrum, but there the  $H\beta$  and [OIII] doublet are absent (they would not have been within the wavelength coverage for CNOC). The CNOC redshift is supported by its membership in the galaxy cluster, and thus it is likely that this galaxy is an example of a strong [OII] emitter which we would have flagged as a problem (quality flag 2).

SPS J162341.40+263433.0 – The continuum may be contaminated by another object along  $x$ . This object has previously been reported by Ellingson et al. (1997) to be a likely member of the  $z=0.4275$  cluster MS1621.5+2640. There is a strong line in the spectrum that we interpret as  $H\alpha$  at  $z=0.369$ . If the cluster redshift were accurate, that line would be

[OI]6300, but no [OIII] or  $H\beta$  would be present in the spectrum.

SPS J164042.82+463843.1 – This spiral galaxy shows stronger line emission from the lower arm than the nucleus.

SPS J171605.64+670411.9 – The direct image of this galaxy shows strong continuum emission from a regular, S0 type morphology, but connected to a fainter “loop”. Likely  $H\alpha$  emission is seen both in the galaxy and faintly in the loop. The morphology is suggestive of an interaction.

SPS J201756.69-704702.1 – This object is a low redshift spiral with many knots. At least one knot has a clearly detectable emission line, most likely  $H\alpha$ .

SPS J204757.09-194653.3 – This object shows strong [OIII] emission but relatively weak Balmer emission, suggestive of an AGN. The direct image is only marginally resolved (FWHM = 2.8 pixels).

SPS J204757.58-194718.3 – This huge spiral galaxy has at least 15 distinct knots in the direct image, most showing  $H\alpha$  emission in the spectrum. The inferred redshift of  $z = 0.111$  is consistent within the uncertainty with the previously reported value of  $z = 0.11526$  ( De Carvalho et al. 1997).

SPS J224025.90-054736.3 – This object appears to have three nuclei, with line emission clearly visible from all three in the dispersed image.

SPS J224015.89-055449.7 – This spiral galaxy has at least ten knots of continuum emission, some of which also show clear  $H\alpha$  emission.

SPS J235158.92+243041.4 – This spectacular spiral has many knots in the direct image, some of which show probable  $H\alpha$  emission.

## 4.2. Notes On Individual Fields

J094317.0+465333.3 – This field represents a surprising non-detection. The field is located near the  $z=0.41$  cluster Abell 0851, and contains a candidate cluster member from the [OII] emission-line search conducted by Martin et al. (2000). The wavelength of redshifted [OII] at  $z=0.41$  is not accessible to the SPS, but the candidate object shows no [OIII],  $H\beta$ , or  $H\alpha$  emission in the SPS spectrum. The on-band flux excess of the Martin et al. candidate would have been  $\sim 3\sigma$  in the spectrum. The morphology of the object is extremely irregular, and the galaxy covers many pixels. If the line emission is not primarily from a single hotspot it is likely that the emission lines are too faint to be detected in the spectrum.

J123630.1+621745.5 – This field is one of the deepest STIS parallels. Chen et al. (1999, 2000) searched this field for high redshift Ly $\alpha$ -emitters, but none were conclusively detected (see also Stern et al. 2000). We only detect two emission line objects at  $z \lesssim 1$ .

## 5. Discussion

The deep SPS fields cover 160 square arcminutes (with 141 square arcminutes of usable area) along 219 distinct lines of sight. 131 objects with emission lines were identified. Forty-four fields have multiple emission line objects. Emission-line redshifts are inferred ranging from  $z=0.034$  to  $z=1.548$ . Seventy-eight objects are identified as having [OII] emission, of which 13 also have other emission lines. Forty objects are identified primarily with H $\alpha$  emission, and 13 with [OIII] or H $\beta$  in the absence of H $\alpha$  and [OII]. Of these, 37 have secure redshifts (multiple lines; quality 4), 25 have quality 3, 28 have poor redshifts (quality 1), 15 have problem redshifts (quality 1.5 or 2), and 26 appear to have H $\alpha$  emission for which we do not measure line fluxes.

Figure 25 shows the distribution of inferred redshifts. The detection of objects falls off at the edges of the wavelength range as the sensitivity drops. At the lowest redshifts, the falloff in H $\alpha$  objects is attributable to the small volume covered by the survey. Figure 26 shows the distribution of apparent magnitude.

A rough calculation of the density of detected objects can be made by considering the [OII]-emitters detected at the redshifts that place the [OII] line in the good regions of the sensitivity curve, ( $0.5 < z < 1.2$ ). The SPS surveys a comoving volume of  $1.62 \times 10^5 h_{50}^{-3}$  Mpc $^3$  for  $\Omega_M = 1, \Omega_\Lambda = 0$  (or  $1.56 \times 10^5 h_{70}^{-3}$  Mpc $^3$  for  $\Omega_M = 0.3, \Omega_\Lambda = 0.7$ ) between those redshifts, and detects 63 [OII]-emitters, giving a comoving number density of  $3.7 \times 10^{-4} h_{50}^{-3}$  Mpc $^{-3}$ . This density is slightly higher than that detected by the NICMOS parallels at  $0.7 < z < 1.9$  (McCarthy et al. 1999). As McCarthy et al. (1999) point out, this density is lower than the density of galaxies brighter than  $L^*$  today (Ellis et al. 1996), not all of which are star-forming, but is comparable to that of Lyman Break Galaxies at  $z \sim 3$  (Steidel et al. 1996). The SPS sample of [OII] emitters is sufficient to measure the comoving star-formation density at a median  $z \sim 0.9$ , and we will present that analysis in Paper II.

The SPS fields provide promising results for the detection of intermediate redshift galaxies in optical slitless spectroscopy of random fields. While the survey is subject to a number of biases (towards compact objects and away from low equivalent width lines), it is an efficient means to detect distant, faint galaxies. The high resolution of the direct images should also enable a study of the morphological properties of intermediate redshift galaxies. The

installation of the Advanced Camera for Surveys (ACS; Ford et al. 2001) on HST will make a more extensive survey possible in the coming years. With its larger field of view and filtered imaging capabilities, ACS will refine the procedures developed for the SPS program.

We thank the members of the Space Telescope Imaging Spectrograph Investigation Definition Team (STIS IDT) for their encouragement of this project. In particular, we acknowledge the contribution of Terry Beck, Ruth Bradley, Keith Feggans, Theodore R. Gull, Mary E. Kaiser, Philip C. Plait, Jennifer L. Sandoval, and Gerard M. Williger. This research has made use of the NASA/IPAC Extragalactic Database (NED), which is operated by the Jet Propulsion Laboratory, California Institute of Technology, under contract with the National Aeronautics and Space Administration.

Funding for this publication was provided by NASA through Proposal number HST-AR-08380 submitted to the Space Telescope Science Institute, which is operated by the Association of Universities for Research in Astronomy, Inc., under NASA contract NAS5-26555. Support was also provided by the STIS IDT through the National Optical Astronomical Observatories and by the Goddard Space Flight Center. J.R. was supported by the National Research Council-GSFC Research Associateship.

## REFERENCES

- Baum, S., et al. 1996, STIS Instrument Handbook, Version 1.0 (Baltimore, STScI)
- Becker, R. H., White, R. L., & Helfand, D. J. 1995, *ApJ*, 450, 559
- Bertin, E. & Arnouts, S. 1996, *A&AS*, 117, 393
- Chen, H.-W., Lanzetta, K. M., & Pascarelle, S. 1999, *Nature*, 398, 586
- Chen, H.-W., Lanzetta, K. M., Pascarelle, S., & Yahata, N. 2000, *Nature*, 408, 562
- Cohen, J. G., Hogg, D. W., Blandford, R., Cowie, L. L., Hu, E., Songaila, A., Shopbell, P., & Richberg, K. 2000, *ApJ*, 538, 29
- Cristiani, S., et al. 2000, *A&A*, 359, 489
- De Carvalho, R. R., Ribeiro, A. L. B., Capelato, H. V., & Zepf, S. E. 1997, *ApJS*, 110, 1
- Dressler, A., & Gunn, J. E. 1992, *ApJS*, 78, 1
- Ellingson, E., Yee, H. K. C., Abraham, R. G., Morris, S. L., Carlberg, R. G., & Smecker-Hane, T. A. 1997, *ApJS*, 113, 1
- Ellis, R. S., Colless, M., Broadhurst, T., Heyl, J., & Glazebrook, K. 1996, *MNRAS*, 280, 235

- Ford, H. C.; Advanced Camera for Surveys Science Team 2001, BAAS, 199.0802
- Gardner, J.P., et al. 1998, ApJ, 492, L99
- Giacconi, R., et al. 2002, ApJS, 139, 369
- Godwin, Metcalfe, & Peach 1983, MNRAS, 202, 113
- Griffiths, R.E., et al. 1994, ApJ, 435, L19
- Gruppioni, C., Zamorani, G., De Ruiter, H. R., Parma, P., Mignoli, M., & Lari, C. 1997, MNRAS, 286, 470
- Hammer, F., et al. 1997, ApJ, 481, 49
- Hu, E. M., McMahon, R. G., & Egami, E. 1996, ApJ, 459, L53
- Infante, L., Pritchett, C. J., & Hertling, G. 1995, Journal of Astronomical Data, 1, 2
- Izotov, Y. I., Thuan, T. X., Lipovetsky, V. A. 1994, ApJ, 435, 647
- Kennicutt, R.C., Jr. 1992, ApJ, 338, 310
- Kennicutt, R. C., Jr. 1998, ARA&A, 36, 189
- Kimble, R.A., et al. 1998, ApJ, 492, L83
- Kobulnicky, H.A., Kennicutt. R.C. Jr., & Pizagno, J.L. 1999, ApJ 514, 544
- Maddox, S. J., Sutherland, W. J., Efstathiou, G., & Loveday, J. 1990, MNRAS, 243, 692
- Margoniner, V., & De Carvalho, R. 2000, AJ, 119, 1562
- Martin, C., Lotz, J., & Ferguson, H. 2000, ApJ, 543, 97
- McCarthy, P.J., et al. 1999, ApJ, 520, 548
- Oort, M. 1987, A&AS, 71, 221
- Pettini, M., Shapley, A.E., Steidel, C.C., Cuby, J.-G., Dickinson, M., Moorwood, A.F.M., Adelberger, K.L., & Giavalisco, M. 2001, ApJ, 554, 981
- Steidel, C.C., Giavalisco, M., Pettini, M., Dickinson, M., & Adelberger, K.L., 1996, ApJ Letters 462, L17
- Stern, D., Eisenhardt, P., Spinrad, H., Dawson, S., van Breugel, W., Dey, A., de Vries, W., & Stanford, S.A. 2000, Nature, 408, 560
- Storrie-Lombardi, L. J., McMahon, R. G., Irwin, M. J., & Hazard, C. 1996, ApJ, 468, 121
- Teplitz, H.I., et al. 2000, ApJ, 533, L65
- Teplitz, H.I., Collins, N.R., Gardner, J.P., Hill, R.S., & Rhodes, J. 2002 submitted
- Terlevich, R., Melnick, J., Masegosa, J., Moles, M., Copetti, M. V. F. 1991, A&AS, 91, 285

Thompson, R. I., Rieke, M., Schneider, G., Hines, D. C., & Corbin, M. R. 1998, *ApJ*, 492, L95

Williams, R.E., et al. 1996, *AJ*, 112, 1335

Yan, L., McCarthy, P.J., Freudling, W., Teplitz, H.I., Malumuth, E.M., & Weymann, R.J., Malkan, M.A. 1999, *ApJ*, 519, L47

Table 1. Deep SPS Fields

$\alpha(2000)$	$\delta(2000)$	Img. Exptime (s)	Sp. Exptime (s)	$1\sigma$ flux <sup>1</sup>	area (sq. arcmin.)
00 16 2.0	+15 47 9.5	600	3638	5	0.63
00 16 27.9	+16 01 46.9	600	3631	5	0.43
00 17 17.1	+16 02 20.8	600	3630	4	0.64
00 17 26.8	+15 48 8.2	600	3632	5	0.64
00 37 25.7	+09 07 28.9	1350	5239	19	0.55
00 38 4.3	+13 18 11.8	1700	4284	5	0.58
01 00 31.9	-33 28 21.6	1200	7200	4	0.67
01 03 29.8	+13 15 15.3	7296	4953	4	0.64
01 04 13.4	+21 51 47.7	4634	5391	5	0.67
01 07 36.9	+16 36 35.3	1400	3507	5	0.67
01 37 58.5	-24 30 34.9	2200	5562	4	0.67
02 10 48.6	-39 33 26.1	1668	5071	5	0.63
02 28 5.1	+00 42 36.1	700	3384	8	0.67
02 28 26.6	-01 14 29.4	1000	4362	6	0.67
02 28 33.7	+01 19 15.2	736	3546	11	0.67
02 35 25.4	+03 51 50.1	600	3600	6	0.67
02 36 21.0	+06 50 31.1	600	3600	5	0.67
02 40 29.5	-01 34 35.5	600	3600	5	0.65
02 40 30.4	-01 36 33.3	1450	6000	4	0.67
02 40 31.7	-01 35 41.9	900	5400	5	0.67
02 42 5.0	-34 02 1.4	1200	7200	4	0.67
03 02 10.9	+00 11 55.3	300	3321	6	0.65
03 02 20.8	+00 11 53.9	300	3326	6	0.65
03 02 30.8	+00 12 12.6	300	3294	7	0.66
03 12 40.6	-55 25 36.9	1250	4247	4	0.44
03 13 9.1	-55 25 21.1	2921	3384	4	0.50
03 13 53.8	-55 01 14.1	2600	3440	4	0.53
03 14 1.8	-55 25 8.4	600	4500	5	0.57
03 14 20.3	-54 55 21.9	600	4500	4	0.65
03 14 40.6	-55 06 17.4	1550	5382	4	0.52
03 15 24.2	-55 39 9.5	1550	5382	4	0.61
03 15 47.8	-55 15 35.1	3042	4580	4	0.46
03 20 21.5	+15 29 12.8	1300	6678	7	0.66
03 24 20.4	-36 28 16.4	1400	3448	5	0.67
03 28 49.9	+03 00 51.3	1580	7385	4	0.67
03 31 44.8	-27 44 57.4	3900	3386	6	0.67
03 31 49.9	-27 41 24.4	2700	3602	5	0.66
03 32 6.0	-27 44 15.4	3900	3497	5	0.66
03 41 36.2	-44 55 32.4	1976	8961	4	0.66
03 42 4.7	-29 50 49.0	4800	31800	5	0.64
03 54 31.0	-49 39 32.8	3200	16677	3	0.63
03 59 51.1	-44 30 41.4	450	3290	5	0.67
04 14 21.2	+04 14 3.3	1350	4973	8	0.67
04 24 26.6	+02 00 48.1	603	3884	5	0.67
04 54 35.1	-53 25 14.6	11100	7777	4	0.67
05 46 24.6	-51 08 6.1	450	3392	5	0.67
08 18 44.1	+56 50 29.8	1200	4864	4	0.65
08 19 31.6	+70 50 21.3	1900	3000	9	0.63

Table 1—Continued

$\alpha(2000)$	$\delta(2000)$	Img. Exptime (s)	Spc. Exptime (s)	$1\sigma$ flux <sup>1</sup>	area (sq. arcmin.)
08 23 45.7	+29 23 43.2	600	6000	5	0.66
08 28 36.8	+34 37 56.0	1400	3226	6	0.67
08 37 33.7	+69 50 47.2	5834	4923	6	0.67
08 42 2.5	+70 42 39.2	1900	3000	9	0.65
08 48 38.2	+44 48 37.5	1500	13578	3	0.55
08 49 3.3	+44 52 45.7	4350	4432	45	0.56
08 49 5.2	+44 50 17.9	6300	3591	7	0.67
08 49 10.7	+37 26 12.1	700	3000	9	0.58
08 49 14.9	+44 54 59.2	3250	3216	6	0.59
09 19 43.1	+33 40 21.8	900	4167	6	0.67
09 22 13.6	+50 51 25.4	3700	11606	4	0.67
09 27 0.0	-05 34 1.0	750	4467	5	0.67
09 28 6.6	-05 05 4.5	603	4045	5	0.64
09 28 30.2	-05 01 26.1	2250	14252	3	0.66
09 31 28.4	-04 41 55.0	2723	3656	5	0.67
09 33 39.5	+55 09 39.6	1200	7266	3	0.67
09 43 15.0	+48 08 18.7	2250	11164	4	0.64
09 43 16.9	+46 56 3.3	600	3036	11	0.66
09 43 17.0	+46 53 33.3	600	3153	5	0.64
09 45 54.6	-08 41 24.2	635	4523	5	0.67
09 48 10.0	+13 11 50.0	450	4410	5	0.67
09 52 37.1	+43 58 36.3	2603	5696	4	0.66
09 56 18.3	+69 45 37.0	1300	4800	5	0.66
09 56 23.8	+69 45 40.6	1050	6000	5	0.67
09 56 30.3	+47 29 8.9	1500	7158	4	0.67
09 57 6.6	+69 36 48.7	867	3838	4	0.65
10 00 52.8	+25 08 36.6	1800	3162	5	0.66
10 07 41.9	+10 20 45.9	1450	5830	5	0.67
10 20 50.7	+36 52 10.6	606	3902	5	0.67
10 24 28.3	+47 13 31.3	1650	3147	5	0.67
10 24 28.3	+47 13 31.7	2150	11213	3	0.67
10 35 47.9	-03 41 34.4	900	3600	5	0.61
10 35 49.8	-03 41 21.4	900	3600	5	0.68
10 36 41.0	-03 47 12.5	1547	7317	4	0.66
10 38 58.2	+41 46 45.7	5200	21000	15	0.54
10 46 42.7	-00 12 18.7	2200	4098	5	0.66
10 54 5.8	-03 43 53.0	1609	7412	5	0.62
10 54 32.8	-03 38 56.9	610	3232	5	0.67
10 54 32.9	-03 39 47.0	472	3380	5	0.67
10 56 24.7	-04 19 34.4	1515	9353	4	0.65
10 56 54.8	-03 42 58.5	2268	4010	5	0.66
10 56 59.4	-03 44 8.2	3388	4861	5	0.61
10 56 59.6	-03 40 38.2	3388	4799	5	0.59
10 57 4.2	-03 41 47.3	2618	4001	5	0.66
10 57 8.9	-03 42 57.7	3788	4925	5	0.67
10 57 25.9	-03 38 12.1	756	4464	5	0.63
10 57 31.1	-03 19 2.8	1359	8132	4	0.67
10 57 58.1	-03 14 16.5	1095	3306	5	0.68

Table 1—Continued

$\alpha(2000)$	$\delta(2000)$	Img. Exptime (s)	Spc. Exptime (s)	$1\sigma$ flux <sup>1</sup>	area (sq. arcmin.)
11 01 38.4	-12 11 23.4	300	3516	5	0.67
11 03 34.7	+34 44 46.6	1247	5550	7	0.67
11 18 23.4	+58 52 1.5	1437	9868	4	0.67
11 18 24.3	+07 41 28.9	450	3796	18	0.66
11 20 58.0	+23 23 14.0	1200	7769	4	0.66
11 20 58.4	+23 25 0.2	2708	3863	5	0.67
11 33 37.7	+04 10 46.0	2723	3656	5	0.66
11 39 47.2	+66 03 54.2	1700	4889	5	0.67
11 39 50.6	+66 03 36.8	1440	9094	4	0.67
11 44 13.3	+19 52 23.9	1050	3522	7	0.67
11 45 6.9	+49 47 13.4	900	9363	4	0.64
11 56 14.0	+55 02 27.0	1050	3532	5	0.62
11 56 17.3	+65 19 36.9	1550	4630	4	0.64
11 56 21.4	+55 02 7.8	7610	42517	6	0.74
11 58 14.7	+43 53 1.2	700	3322	7	0.42
12 01 14.7	-18 56 25.1	5100	6059	5	0.66
12 05 23.1	-07 42 33.5	2160	11317	3	0.75
12 13 41.5	+17 14 2.1	1650	10424	5	0.66
12 17 17.2	-03 15 49.2	1000	3320	8	0.67
12 19 3.9	+47 08 20.6	4070	12279	3	0.67
12 26 27.2	+31 07 34.2	1550	5096	13	0.67
12 28 23.1	+12 36 22.4	2785	8038	4	0.67
12 28 34.5	+02 07 25.1	12762	7206	4	0.61
12 30 20.2	+12 28 55.0	900	4800	6	0.67
12 30 28.1	+12 31 46.2	850	3217	5	0.65
12 31 0.8	+12 14 20.7	1700	7518	6	0.67
12 31 1.3	+12 14 18.3	1800	4722	17	0.67
12 31 1.7	+12 14 16.1	1750	8517	6	0.67
12 31 4.1	+12 14 38.6	3167	6778	7	0.63
12 31 9.2	+12 16 0.1	753	5781	4	0.67
12 33 47.9	+02 32 0.7	900	4991	6	0.64
12 34 2.2	+02 49 26.2	820	5204	9	0.66
12 34 10.9	+02 33 39.9	10200	51140	3	0.61
12 36 30.1	+62 17 45.5	13400	48600	2	0.64
12 37 3.6	+14 08 2.2	3350	17033	3	0.67
12 42 10.7	+32 27 27.4	2043	7699	5	0.67
12 48 5.9	+34 29 28.7	4649	8959	5	0.67
12 50 55.3	+10 50 48.4	1000	3975	5	0.67
12 59 17.0	+36 27 8.7	600	3548	5	0.67
12 59 41.5	+36 12 17.1	647	3522	7	0.54
13 00 3.2	+27 53 53.5	1848	10764	4	0.67
13 00 15.1	+27 54 1.7	1546	7410	7	0.67
13 01 58.6	+27 32 45.3	4400	20654	3	0.66
13 05 39.2	+36 43 46.4	750	3870	4	0.65
13 08 45.5	+29 11 11.7	1050	3315	6	0.64
13 08 59.9	+29 20 34.4	450	3740	6	0.67
13 09 5.6	+29 21 50.1	700	3422	6	0.67
13 09 27.4	+29 22 40.0	600	3617	4	0.64

Table 1—Continued

$\alpha(2000)$	$\delta(2000)$	Img. Exptime (s)	Spc. Exptime (s)	$1\sigma$ flux <sup>1</sup>	area (sq. arcmin.)
13 09 45.8	+32 17 28.1	1200	5023	4	0.65
13 11 17.3	-01 18 28.6	450	3774	24	0.61
13 12 55.6	-19 26 25.6	1450	5622	7	0.64
13 18 11.5	-00 04 51.3	750	4861	6	0.67
13 25 9.0	+30 14 33.0	2150	6808	4	0.67
13 25 43.1	-11 31 57.7	850	4056	6	0.66
13 30 8.3	+47 07 33.7	750	4546	15	0.67
13 40 36.6	+27 34 30.7	600	6000	4	0.67
13 43 23.8	+02 15 54.8	606	3821	6	0.64
13 43 31.1	+01 18 20.6	427	3001	6	0.52
13 43 40.2	+01 22 2.2	606	3768	5	0.66
13 44 29.0	-00 09 35.9	1700	5527	46	0.61
13 46 7.2	+01 59 13.3	606	3709	5	0.67
13 47 22.1	+02 13 46.8	427	3001	6	0.57
13 47 29.8	+02 17 50.6	606	3764	5	0.67
13 47 54.3	+07 46 40.1	2307	6570	4	0.67
13 52 59.0	+31 29 13.9	1450	5212	6	0.48
14 00 50.4	+62 19 30.7	600	4494	4	0.56
14 01 41.7	+15 08 48.5	1744	5678	5	0.67
14 15 47.3	+52 03 39.1	1098	4104	5	0.63
14 18 26.8	+52 34 16.9	900	5400	4	0.57
14 24 26.8	+23 00 6.3	1300	5943	4	0.67
14 29 52.7	+42 05 12.4	710	3570	5	0.65
14 29 56.3	+42 07 20.4	600	6000	4	0.49
14 41 30.9	+53 24 35.0	2700	16200	4	0.61
14 44 50.5	+38 45 11.9	450	4252	5	0.67
14 50 41.4	+63 14 31.6	600	4306	4	0.68
15 08 18.3	+02 32 43.7	753	5912	5	0.67
15 14 21.4	+36 52 46.4	1713	5610	5	0.63
15 16 15.6	-00 13 24.4	1750	5712	10	0.64
15 16 51.9	+06 56 48.2	1500	9000	5	0.67
15 39 48.2	+66 08 54.5	428	3407	23	0.67
15 50 4.9	+21 23 19.9	900	5400	4	0.67
15 50 5.2	+21 20 59.7	900	5400	5	0.61
16 02 5.0	+43 14 47.0	850	4688	18	0.67
16 04 44.2	+43 26 9.4	2900	12600	3	0.67
16 09 58.7	+65 33 55.3	2400	14400	3	0.55
16 11 7.9	+14 51 59.9	4350	11325	5	0.68
16 23 42.6	+26 34 35.6	750	5086	11	0.68
16 23 57.1	+26 28 5.2	1550	5394	13	0.65
16 24 43.3	+23 40 58.5	5900	3476	5	0.67
16 25 13.3	+23 48 58.1	1950	3000	7	0.69
16 32 18.0	+37 28 43.5	600	3342	4	0.67
16 40 43.1	+46 38 59.7	1600	10157	3	0.65
16 44 34.3	+23 42 19.7	600	3000	16	0.58
16 45 31.0	+46 23 25.0	2183	6614	17	0.68
16 49 6.7	+60 14 15.4	600	6660	4	0.68
17 01 28.4	+64 15 58.0	837	4932	4	0.66

Table 1—Continued

$\alpha(2000)$	$\delta(2000)$	Img. Exptime (s)	Spc. Exptime (s)	$1\sigma$ flux <sup>1</sup>	area (sq. arcmin.)
17 16 7.4	+67 04 17.7	1860	8707	5	0.67
17 22 42.9	+50 00 28.9	600	3600	5	0.62
17 23 21.3	+50 01 17.4	1080	4320	5	0.82
20 17 57.9	-70 46 58.3	5364	8057	5	0.66
20 47 56.6	-19 46 59.0	2850	10861	5	0.60
20 50 51.2	-57 05 3.4	303	3121	8	0.67
22 05 29.8	+13 02 28.7	1244	5084	8	0.59
22 17 48.3	+00 13 6.2	2500	4970	4	0.67
22 32 3.6	+02 43 15.7	903	8645	5	0.60
22 40 14.6	-05 54 52.0	1623	10746	5	0.64
22 40 24.1	-05 48 3.2	900	3600	5	0.66
22 40 24.9	-05 47 34.0	900	3600	5	0.66
22 46 32.6	-00 47 25.3	750	4642	7	0.67
22 53 15.4	-14 25 26.9	3350	24612	5	0.43
23 12 33.0	+00 59 35.3	450	3840	6	0.67
23 12 37.7	+00 58 25.4	450	3775	8	0.67
23 13 4.5	+00 53 34.5	712	3785	6	0.67
23 13 4.5	+00 51 14.5	604	3507	6	0.67
23 17 43.8	-04 36 59.9	750	3595	14	0.66
23 24 36.2	+28 04 6.2	592	3649	14	0.59
23 29 25.4	+00 09 29.9	300	3750	6	0.67
23 48 41.8	+00 56 48.7	6150	6011	4	0.64
23 50 38.0	+27 10 4.6	900	8910	7	0.66
23 51 57.9	+24 30 22.7	2826	10913	4	0.61
02 34 58.0	+03 34 56.0	300	3600	5	0.66
12 35 24.2	+62 14 32.4	2950	7200	4	0.61
12 35 24.7	+62 14 55.8	2950	7200	4	0.66

<sup>1</sup>( $10^{-17}$  erg cm<sup>-2</sup> s<sup>-1</sup>)

Table 2. NED Objects in the Deep SPS Fields

$\alpha(2000)$	$\delta(2000)$	NED Objects	ref. <sup>1</sup>
03 12 40.6	-55 25 36.9	APMUKS(BJ) B031118.74-553640.9	1
03 13 53.8	-55 01 14.1	[GZd97] 1.4GHz 20 & 21	2
03 14 1.8	-55 25 8.4	APMUKS(BJ) B031242.66-553605.6	1
03 14 40.6	-55 06 17.4	APMUKS(BJ) B031319.21-551732.9	1
03 32 6.0	-27 44 15.4	CDF-S <sup>2</sup> EIS U21; z=3.462	3
08 48 38.2	+44 48 37.5	65W 106	4
08 49 10.7	+37 26 12.1	FIRST J084910.4+37263	5
09 43 16.9	+46 56 3.3	ABELL 0851:[DG92] 044	6
09 43 17.0	+46 53 33.3	ABELL 0851:[MLF2000] 0756	7
10 56 24.7	-04 19 34.4	APMUKS(BJ) B105350.62-040334.8	1
12 05 23.1	-07 42 33.5	QSO 2MASSi J1205231-07423 (z=4.694) <sup>3</sup>	8
12 36 30.1	+62 17 45.5	HDF adjacent <sup>4</sup>	...
13 00 15.1	+27 54 1.7	ABELL 1656:[GMP83] 2808 & 2835	9
13 08 45.5	+29 11 11.7	NGPFG 03247 & 05987	10
13 08 59.9	+29 20 34.4	NGPFG 04214,55512,05776, 08918,05777	10
13 09 5.6	+29 21 50.1	NGPFG 59295,08840,55461,08824, 48290	10
13 09 27.4	+29 22 40.0	NGPFG 08582, 04413,05510,04421,04405,04390,05521,04442	10
13 11 17.3	-01 18 28.6	Abell 1689 adjacent <sup>5</sup>	1,11
13 43 31.1	+01 18 20.6	APMUKS(BJ) B134057.62+013313.7, B134058.48+013347.0	1
16 23 42.6	+26 34 35.6	MS 1621.5+2640:[EYA97] 101200,101286,101376,101302, 101148,101311	12
16 23 57.1	+26 28 5.2	MS 1621.5+2640:[EYA97] 301086 z=0.47473	12
20 47 56.6	-19 46 59.0	HCG 087:[dRC97] 18 z=0.11526	13

<sup>1</sup> 1 – Maddox et al. (1990); 2 – Gruppioni et al. (1997); 3 – Cristiani et al. (2000);  
4 – Oort (1987); 5 – Becker et al. (1995); 6 – Dressler & Gunn (1992);  
7 – Martin et al. (2000); 8 – Storrie-Lombardi et al. (1996); 9 – Godwin et al. (1983);  
10 – Infante et al. (1995); 11 – Margoniner & De Carvalho (2000); 12 – Ellingson et al. (1997);  
13 – De Carvalho et al. (1997)

<sup>2</sup>This field is a few arcminutes from the center of the Chandra Deep Field South (Giacconi et al. 2002).

<sup>3</sup>This field was included in the Hu et al. (1996) Lyman- $\alpha$  search for quasar companions.

<sup>4</sup>This field, parallel to the Hubble Deep Field North (Williams et al. 1996) was analyzed independently by Chen et al. (1999,2000) and Stern et al. (2000).

<sup>5</sup>This field contains: APMUKS(BJ) B130842.46-010229.8, B130844.25-010243.7 (z=0.209498), [MD2000] J131117.984-011812.47, [MD2000] J131118.783-011843.00, [MD2000] J131119.214-011830.18

Table 3. Detected Objects

obj name	$\alpha(2000)$	$\delta(2000)$	Redshift <sup>1</sup>	z flag <sup>2</sup>	50CCD <sup>3</sup>	FWHM (arcsec)	a/b	P.A. (deg.)	$\lambda$ range (Å)	Strong Lines Detected
SPS J001716.56+160239.5	00:17:16.56	16:02:39.5	1.074	1	25.03 ± 0.09	0.45	1.0	-85	6343-10000	[OII]
SPS J010030.43-332823.4	01:00:30.43	-33:28:23.4	0.702	3	24.61 ± 0.05	1.34	1.7	-40	5300-8467	[OII]
SPS J010329.80+131508.9	01:03:29.80	13:15:08.9	0.819	4	22.64 ± 0.03	0.33	1.2	-27	5392-10000	[OII]-H $\delta$ -H $\gamma$ -H $\beta$ -[OIII]
SPS J021048.23-393308.0	02:10:48.23	-39:33:08.0	0.593	2	26.17 ± 0.08	0.38	1.2	37	5300-8598	[OII]
SPS J022828.08-011434.0	02:28:28.08	-01:14:34.0	0.151	0	21.14 ± 0.03	2.79	1.8	45	7123-10000	H $\alpha$
SPS J030221.47+001150.6 <sup>4</sup>	03:02:21.47	00:11:50.6	0.920	3	24.41 ± 0.09	0.97	1.9	-19	5300-9180	[OII]
SPS J030210.18+001140.0 <sup>4</sup>	03:02:10.18	00:11:40.0	1.092	1	25.20 ± 0.13	0.45	1.3	50	5375-10000	[OII]
SPS J031357.20-550113.5	03:13:57.20	-55:01:13.5	0.688	3	23.13 ± 0.03	0.72	1.3	62	5300-8445	[OII]
SPS J032022.38+152854.1	03:20:22.38	15:28:54.1	1.344	1	24.12 ± 0.04	0.39	1.1	-83	7227-10000	[OII]
SPS J033146.65-274453.5	03:31:46.65	-27:44:53.5	0.707	3	25.14 ± 0.04	1.48	1.6	-55	5300-8187	[OII]
SPS J033144.66-274518.7	03:31:44.66	-27:45:18.7	0.217	0	20.57 ± 0.03	0.46	1.4	63	5300-9738	[OIII]-H $\alpha$
SPS J035431.21-493924.0	03:54:31.21	-49:39:24.0	0.828	4	24.69 ± 0.03	0.20	1.0	79	5300-9773	[OII]-H $\beta$ -[OIII]
SPS J035430.34-493914.3	03:54:30.34	-49:39:14.3	0.227	0	20.96 ± 0.03	0.87	2.0	60	5300-10000	H $\alpha$
SPS J041420.84+041417.6	04:14:20.84	04:14:17.6	1.028	1	23.86 ± 0.03	1.89	1.4	-39	5300-8852	[OII]
SPS J045437.34-532514.1	04:54:37.34	-53:25:14.1	0.357	1	22.88 ± 0.03	0.37	1.4	24	6541-10000	H $\alpha$
SPS J082344.12+292351.3	08:23:44.12	29:23:51.3	0.147	4	24.40 ± 0.05	0.16	1.0	-73	5300-8961	H $\beta$ -[OIII]-H $\alpha$
SPS J082346.66+292323.3	08:23:46.66	29:23:23.3	1.324	1	25.46 ± 0.17	0.50	1.2	79	7389-10000	[OII]
SPS J084837.09+444819.8	08:48:37.09	44:48:19.8	0.644	4	21.67 ± 0.03	0.13	1.1	83	6814-10000	H $\beta$ -[OIII]
SPS J084837.63+444845.3	08:48:37.63	44:48:45.3	0.841	3	23.98 ± 0.03	1.72	1.2	44	5300-9419	[OII]
SPS J084840.29+444845.8	08:48:40.29	44:48:45.8	0.348	4	21.31 ± 0.03	3.35	1.6	-81	5300-9651	H $\beta$ -H $\beta$ -[OIII]-H $\alpha$
SPS J084904.39+445308.5	08:49:04.39	44:53:08.5	0.423	4	25.02 ± 0.03	0.12	1.0	-56	5300-8736	H $\beta$ -[OIII]
SPS J084916.65+445457.7	08:49:16.65	44:54:57.7	1.528	1	26.00 ± 0.10	0.78	1.3	-3	6874-10000	[OII]
SPS J092658.16-053358.8	09:26:58.16	-05:33:58.8	0.075	0	20.34 ± 0.03	2.22	3.0	-47	5300-8225	H $\alpha$
SPS J092829.86-050121.9	09:28:29.86	-05:01:21.9	0.904	3	24.78 ± 0.03	0.23	1.1	67	5300-9659	[OII]
SPS J092830.13-050118.6	09:28:30.13	-05:01:18.6	1.350	1	23.39 ± 0.03	0.33	1.0	20	5300-9540	[OII]
SPS J093340.07+550951.3	09:33:40.07	55:09:51.3	0.556	4	24.34 ± 0.03	0.21	1.0	48	5300-9042	[OII]-H $\beta$ -[OIII]
SPS J094810.95+131142.6	09:48:10.95	13:11:42.6	0.950	1.5	24.38 ± 0.06	0.95	1.1	-50	6412-10000	[OII]
SPS J095240.06+435834.9	09:52:40.06	43:58:34.9	0.405	4	23.36 ± 0.03	1.31	1.2	-4	5300-7998	H $\beta$ -[OIII]
SPS J095615.40+694535.3 <sup>5</sup>	09:56:15.40	69:45:35.3	0.782	2	23.42 ± 0.03	2.59	1.9	82	5300-9566	[OII]
SPS J095628.10+694551.9 <sup>5</sup>	09:56:28.10	69:45:51.9	0.233	0	21.95 ± 0.03	2.78	1.2	-17	6952-10000	H $\alpha$
SPS J100051.56+250858.6	10:00:51.56	25:08:58.6	0.663	3	23.32 ± 0.03	0.45	1.2	-18	5300-8024	[OII]
SPS J100051.67+250853.0	10:00:51.67	25:08:53.0	1.138	1	23.80 ± 0.03	1.33	1.3	51	5300-8563	[OII]
SPS J100052.03+250839.2	10:00:52.03	25:08:39.2	1.077	3	25.57 ± 0.08	0.57	1.0	-86	5300-9885	[OII]
SPS J100743.50+102045.7	10:07:43.50	10:20:45.7	0.158	0	19.79 ± 0.03	0.24	1.7	-13	7368-10000	H $\alpha$ -[SII]
SPS J102049.27+365226.3	10:20:49.27	36:52:26.3	0.717	3	22.79 ± 0.03	0.35	1.4	-65	5300-8219	[OII]
SPS J102429.80+471314.2	10:24:29.80	47:13:14.2	0.723	3	24.35 ± 0.03	0.36	1.1	22	5300-8364	[OII]

Table 3—Continued

obj name	$\alpha(2000)$	$\delta(2000)$	Redshift <sup>1</sup>	z flag <sup>2</sup>	50CCD <sup>3</sup>	FWHM (arcsec)	a/b	P.A. (deg.)	$\lambda$ range (Å)	Strong Lines Detected
SPS J103640.31-034708.1	10:36:40.31	-03:47:08.1	0.934	3	24.46 ± 0.03	0.80	1.2	-29	5300-9121	[OII]
SPS J104643.01-001212.7	10:46:43.01	-00:01:12.7	1.164	1	23.14 ± 0.03	0.09	1.0	81	5300-9913	[OII]
SPS J105433.40-033837.3	10:54:33.40	-03:38:37.3	0.110	0	21.43 ± 0.03	3.79	2.5	59	5300-9312	H $\alpha$
SPS J105655.06-034322.8	10:56:55.06	-03:43:22.8	1.101	1	23.09 ± 0.03	0.11	1.0	28	7517-10000	[OII]
SPS J105700.03-034400.9	10:57:00.03	-03:44:00.9	0.322	4	24.05 ± 0.03	1.86	1.3	-41	5300-9488	[OIII]-H $\beta$ -H $\alpha$
SPS J105756.33-031415.7	10:57:56.33	-03:14:15.7	1.205	1	23.49 ± 0.03	0.27	1.1	65	5300-8755	[OII]
SPS J105705.12-034137.2	10:57:05.12	-03:41:37.2	0.395	4	22.87 ± 0.03	2.44	1.3	-87	5300-9199	H $\gamma$ -H $\beta$ -[OIII]-H $\alpha$
SPS J105702.81-034158.3	10:57:02.81	-03:41:58.3	0.320	4	24.29 ± 0.03	1.86	1.6	7	6252-10000	[OIII]-H $\beta$
SPS J105708.69-034310.8	10:57:08.69	-03:43:10.8	0.403	4	23.85 ± 0.03	0.41	1.4	-89	6465-10000	H $\beta$ -[OIII]-H $\alpha$
SPS J105708.06-034320.1	10:57:08.06	-03:43:20.1	1.052	4	22.89 ± 0.03	0.64	1.1	-27	7355-10000	[OII]-H $\gamma$
SPS J110137.18-121131.1	11:01:37.18	-12:11:31.1	0.538	2	25.28 ± 0.15	0.39	1.1	-86	5300-8664	[OII]
SPS J112057.83+232306.6	11:20:57.83	23:23:06.6	1.066	1	23.34 ± 0.03	1.95	1.4	73	5662-10000	[OII]
SPS J113338.51+041031.8	11:33:38.51	04:10:31.8	0.656	2	23.16 ± 0.03	2.36	1.6	61	5300-8676	[OII]
SPS J113950.96+660350.4	11:39:50.96	66:03:50.4	0.906	3	24.07 ± 0.04	0.71	1.2	69	5300-9117	[OII]
SPS J115616.05+550215.4	11:56:16.05	55:02:15.4	1.170	1	22.79 ± 0.03	2.13	1.0	-35	5543-10000	[OII]
SPS J115623.08+550218.1	11:56:23.08	55:02:18.1	0.067	0	20.72 ± 0.03	5.84	1.5	59	5300-8943	H $\alpha$
SPS J115620.02+651935.3	11:56:20.02	65:19:35.3	0.465	0	21.41 ± 0.03	0.48	1.4	25	6236-10000	[OIII]-H $\alpha$
SPS J120113.92-185633.2	12:01:13.92	-18:56:33.2	0.973	4	22.82 ± 0.03	0.51	2.0	23	5300-10000	[OII]-H $\beta$
SPS J120112.82-185622.5	12:01:12.82	-18:56:22.5	1.113	1	23.63 ± 0.03	1.78	1.4	-7	6932-10000	[OII]
SPS J121340.03+171406.2	12:13:40.03	17:14:06.2	0.119	0	21.59 ± 0.03	0.80	2.8	-35	5300-8866	H $\alpha$
SPS J121716.05-031607.0	12:17:16.05	-03:16:07.0	1.249	1	23.97 ± 0.04	1.65	1.3	-43	6210-10000	[OII]
SPS J121901.51+470804.6	12:19:01.51	47:08:04.6	1.425	1	23.40 ± 0.03	0.21	1.4	-1	7187-10000	[OII]
SPS J121904.77+470754.4	12:19:04.77	47:07:54.4	1.479	1	22.99 ± 0.03	1.22	1.6	10	7532-10000	[OII]
SPS J122821.87+123625.3	12:28:21.87	12:36:25.3	1.063	1	23.72 ± 0.03	0.24	1.1	-25	5300-9440	[OII]
SPS J122821.28+123636.9	12:28:21.28	12:36:36.9	0.965	3	25.27 ± 0.05	0.91	1.3	-14	5300-8140	[OII]
SPS J123103.19+121422.6	12:31:03.19	12:14:22.6	0.746	4	23.71 ± 0.03	0.64	1.2	34	5505-10000	[OII]-H $\beta$ -[OIII]
SPS J123100.06+121419.4	12:31:00.06	12:14:19.4	0.248	0	23.05 ± 0.03	1.49	1.3	-37	5300-9878	H $\alpha$
SPS J123102.59+121424.8 <sup>6</sup>	12:31:02.59	12:14:24.8	0.498	0	22.15 ± 0.03	2.88	1.4	-72	5410-10000	H $\beta$ -[OIII]-H $\alpha$
SPS J123108.68+121542.7	12:31:08.68	12:15:42.7	0.958	3	23.76 ± 0.03	0.14	1.0	2	7074-10000	[OII]
SPS J123348.78+023212.4	12:33:48.78	02:32:12.4	0.690	2	23.09 ± 0.03	1.50	1.9	-40	5300-8636	[OII]
SPS J123410.44+023311.7	12:34:10.44	02:33:11.7	1.528	1	23.72 ± 0.03	0.31	1.2	3	7514-10000	[OII]
SPS J123632.10+621758.3	12:36:32.10	62:17:58.3	1.007	1.5	23.91 ± 0.03	0.27	1.1	-77	5816-10000	[OII]
SPS J123702.88+140744.9	12:37:02.88	14:07:44.9	0.623	4	25.05 ± 0.03	0.18	1.0	-34	6517-10000	H $\beta$ -[OIII]
SPS J123705.08+140801.3	12:37:05.08	14:08:01.3	0.419	4	23.46 ± 0.03	0.15	1.1	89	5912-10000	H $\beta$ -[OIII]-H $\alpha$
SPS J123703.08+140803.7	12:37:03.08	14:08:03.7	0.900	4	24.68 ± 0.03	1.62	1.6	-86	5300-9854	[OII]-H $\beta$
SPS J123704.59+140822.5	12:37:04.59	14:08:22.5	1.028	1	23.63 ± 0.03	0.71	1.1	38	5300-8743	[OII]

Table 3—Continued

obj name	$\alpha(2000)$	$\delta(2000)$	Redshift <sup>1</sup>	z flag <sup>2</sup>	50CCD <sup>3</sup>	FWHM (arcsec)	a/b	P.A. (deg.)	$\lambda$ range (Å)	Strong Lines Detected
SPS J124210.24+322744.3	12:42:10.24	32:27:44.3	0.059	0	21.43 ± 0.03	1.01	1.6	4	5300-8595	H $\alpha$
SPS J125055.99+105042.5	12:50:55.99	10:50:42.5	0.821	2	23.01 ± 0.03	0.17	1.2	-64	5300-10000	[OII]
SPS J125054.02+105101.1	12:50:54.02	10:51:01.1	1.337	3	25.88 ± 0.10	0.48	1.3	-15	5300-10000	[OII]
SPS J125917.75+362702.7	12:59:17.75	36:27:02.7	0.356	4	22.09 ± 0.03	0.97	1.1	-38	6113-10000	H $\beta$ -[OIII]-H $\alpha$
SPS J130002.95+275342.0	13:00:02.95	27:53:42.0	0.822	4	23.99 ± 0.03	1.22	1.4	-24	6391-10000	[OII]-[OIII]
SPS J130016.01+275405.5	13:00:16.01	27:54:05.5	0.575	4	24.45 ± 0.03	0.26	1.1	-42	5317-10000	[OII]-H $\beta$ -[OIII]
SPS J130015.23+275336.1	13:00:15.23	27:53:36.1	0.279	0	24.19 ± 0.04	2.20	1.6	22	7580-10000	H $\alpha$
SPS J130927.26+292229.3	13:09:27.26	29:22:29.3	0.760	4	23.03 ± 0.03	0.27	1.1	-5	5898-10000	[OII]-H $\beta$ -[OIII]
SPS J131116.64-011825.5	13:11:16.64	-01:18:25.5	0.079	0	20.84 ± 0.03	5.33	2.2	-42	6154-10000	H $\alpha$
SPS J131812.38-000507.4	13:18:12.38	-00:05:07.4	0.381	4	21.62 ± 0.03	0.23	1.0	57	7269-10000	H $\alpha$ -[SII]
SPS J131810.94-000444.1	13:18:10.94	-00:04:44.1	0.863	3	22.95 ± 0.03	0.32	1.1	-59	5300-9220	[OII]
SPS J131811.71-000434.5	13:18:11.71	-00:04:34.5	0.165	0	22.63 ± 0.03	3.29	1.7	46	5300-9114	H $\alpha$
SPS J131810.43-000453.8	13:18:10.43	-00:04:53.8	3.170	4	21.28 ± 0.03	0.09	1.0	-26	5300-9564	UV lines
SPS J132511.10+301418.3	13:25:11.10	30:14:18.3	0.675	3	23.84 ± 0.03	0.11	1.0	28	5300-8008	[OII]
SPS J133008.55+470741.8	13:30:08.55	47:07:41.8	0.594	4	23.80 ± 0.03	0.23	1.0	65	5300-9728	[OII]-[OIII]
SPS J133006.46+470719.4	13:30:06.46	47:07:19.4	0.960	1.5	23.25 ± 0.03	0.76	1.1	44	5300-10000	[OII]
SPS J134035.18+273417.1	13:40:35.18	27:34:17.1	0.414	4	24.41 ± 0.05	0.21	1.0	49	5726-10000	H $\gamma$ -H $\beta$ -[OIII]
SPS J134322.44+021542.7	13:43:22.44	02:15:42.7	1.480	1	22.83 ± 0.03	0.97	1.6	70	7399-10000	[OII]
SPS J134429.63-000909.6	13:44:29.63	-00:09:09.6	0.181	0	22.32 ± 0.03	1.69	1.9	-66	5300-8249	H $\alpha$
SPS J134606.52+015858.2	13:46:06.52	01:58:58.2	0.756	4	23.05 ± 0.03	1.13	1.6	18	6938-10000	[OIII]-H $\beta$
SPS J134608.36+015922.6	13:46:08.36	01:59:22.6	0.662	3	22.53 ± 0.03	2.84	1.4	-36	5300-8407	[OII]
SPS J134721.93+021407.2	13:47:21.93	02:14:07.2	0.342	4	20.62 ± 0.03	0.21	1.1	1	5610-10000	H $\alpha$ -[OIII]-H $\beta$
SPS J134721.97+021405.7	13:47:21.97	02:14:05.7	0.338	4	23.95 ± 0.06	1.53	2.1	-12	5542-10000	[OIII]
SPS J140051.85+621937.7	14:00:51.85	62:19:37.7	0.074	0	19.26 ± 0.03	5.00	5.0	34	5536-10000	H $\alpha$
SPS J140140.40+150857.3	14:01:40.40	15:08:57.3	0.526	2	24.34 ± 0.03	1.63	1.4	-54	5300-8810	[OII]
SPS J141824.25+523420.0	14:18:24.25	52:34:20.0	0.710	3	23.39 ± 0.03	0.61	1.4	79	5300-7912	[OII]
SPS J142427.43+225959.8	14:24:27.43	22:59:59.8	0.970	3	25.68 ± 0.08	0.32	1.0	17	5300-9229	[OII]
SPS J142957.15+420713.1	14:29:57.15	42:07:13.1	0.568	4	23.94 ± 0.03	0.18	1.0	-32	5300-8983	[OII]-[OIII]
SPS J142955.57+420714.3	14:29:55.57	42:07:14.3	1.080	1	23.21 ± 0.03	1.02	1.9	52	5454-10000	[OII]
SPS J142956.79+420729.4	14:29:56.79	42:07:29.4	0.790	2	26.49 ± 0.14	0.27	1.4	-25	5300-10000	[OII]
SPS J144449.32+384521.1	14:44:49.32	38:45:21.1	0.382	3	21.76 ± 0.03	0.28	1.0	-32	6800-10000	H $\alpha$
SPS J151617.05-001337.9	15:16:17.05	-00:013:37.9	1.268	1	23.76 ± 0.03	2.19	1.4	-41	7491-10000	[OII]
SPS J155003.49+212318.9	15:50:03.49	21:23:18.9	1.183	1	24.15 ± 0.04	0.41	1.3	11	5300-8920	[OII]
SPS J160956.65+653334.6	16:09:56.65	65:33:34.6	0.157	4	20.16 ± 0.03	0.78	1.3	76	5300-8380	H $\beta$ -[OIII]-H $\alpha$
SPS J162357.69+262830.2	16:23:57.69	26:28:30.2	0.090	4	22.21 ± 0.03	1.74	1.0	-45	5300-9055	H $\beta$ -[OIII]-H $\alpha$
SPS J162354.88+262803.5	16:23:54.88	26:28:03.5	0.474	2	22.63 ± 0.03	1.83	2.2	57	5300-8321	[OII]

Table 3—Continued

obj name	$\alpha(2000)$	$\delta(2000)$	Redshift <sup>1</sup>	z flag <sup>2</sup>	50CCD <sup>3</sup>	FWHM (arcsec)	a/b	P.A. (deg.)	$\lambda$ range (Å)	Strong Lines Detected
SPS J162341.40+263433.0	16:23:41.40	26:34:33.0	0.369	2	$22.15 \pm 0.03$	0.87	1.7	85	5300-9301	H $\alpha$
SPS J162444.27+234041.6	16:24:44.27	23:40:41.6	1.360	1	$24.36 \pm 0.03$	0.74	1.2	-83	6849-10000	[OII]
SPS J164042.82+463843.1	16:40:42.82	46:38:43.1	0.223	0	$21.21 \pm 0.03$	1.28	2.2	26	6316-10000	H $\alpha$
SPS J164435.47+234221.2	16:44:35.47	23:42:21.2	0.207	4	$24.04 \pm 0.06$	0.23	1.1	-70	6472-10000	H $\beta$ -[OIII]-H $\alpha$
SPS J164434.54+234207.9	16:44:34.54	23:42:07.9	0.926	1.5	$24.80 \pm 0.10$	0.91	1.3	-19	7065-10000	[OII]
SPS J164908.74+601414.5	16:49:08.74	60:14:14.5	1.189	1	$23.09 \pm 0.03$	0.18	1.0	35	5909-10000	[OII]
SPS J164909.64+601416.3	16:49:09.64	60:14:16.3	1.006	3	$26.23 \pm 0.16$	0.24	1.1	41	6029-10000	[OII]
SPS J171605.64+670411.9	17:16:05.64	67:04:11.9	0.171	0	$21.11 \pm 0.03$	1.14	1.8	50	6327-10000	H $\alpha$
SPS J201756.69-704702.1	20:17:56.69	-70:47:02.1	0.159	0	$22.00 \pm 0.03$	2.68	1.7	-53	5300-10000	H $\alpha$
SPS J204756.29-194709.4	20:47:56.29	-19:47:09.4	0.316	4	$21.43 \pm 0.03$	0.29	1.3	66	5300-9777	H $\beta$ -[OIII]-H $\alpha$
SPS J204757.09-194653.3	20:47:57.09	-19:46:53.3	0.405	4	$22.57 \pm 0.03$	0.14	1.0	48	5300-10000	H $\beta$ -[OIII]-H $\alpha$
SPS J204757.58-194718.3	20:47:57.58	-19:47:18.3	0.111	0	$20.77 \pm 0.03$	5.08	1.2	49	5300-7941	H $\alpha$
SPS J224024.66-054723.3	22:40:24.66	-05:47:23.3	0.619	4	$23.87 \pm 0.03$	0.14	1.0	48	5300-9585	[OII]-H $\beta$ -[OIII]
SPS J224025.90-054736.3	22:40:25.90	-05:47:36.3	0.241	0	$21.55 \pm 0.03$	1.14	1.6	-31	6743-10000	H $\alpha$
SPS J224024.68-054744.5	22:40:24.68	-05:47:44.5	1.141	1	$24.01 \pm 0.04$	1.02	1.5	61	5392-10000	[OII]
SPS J224015.89-055449.7	22:40:15.89	-05:54:49.7	0.278	0	$22.91 \pm 0.03$	0.54	1.3	33	6612-10000	H $\alpha$
SPS J232435.91+280401.8	23:24:35.91	28:04:01.8	0.208	3	$23.32 \pm 0.03$	1.14	1.0	25	5500-10000	H $\alpha$
SPS J232437.59+280404.4	23:24:37.59	28:04:04.4	0.057	0	$21.96 \pm 0.03$	1.60	1.3	58	5300-8380	H $\alpha$
SPS J235036.79+271021.1	23:50:36.79	27:10:21.1	1.548	3	$25.40 \pm 0.13$	0.15	1.0	81	7049-10000	[OII]
SPS J235036.70+271024.2	23:50:36.70	27:10:24.2	1.250	3	$25.58 \pm 0.09$	0.25	1.0	23	7223-10000	[OII]
SPS J235038.34+271003.2	23:50:38.34	27:10:03.2	0.502	2	$24.74 \pm 0.06$	0.59	1.1	-54	5300-9781	[OII]
SPS J235158.16+243036.2	23:51:58.16	24:30:36.2	0.429	4	$23.31 \pm 0.03$	1.76	1.4	52	5300-9268	[OII]-H $\gamma$ -H $\beta$ -[OIII]
SPS J235158.92+243041.4	23:51:58.92	24:30:41.4	0.036	0	$21.71 \pm 0.03$	1.88	2.0	-45	5300-9278	H $\alpha$

<sup>1</sup>The redshift uncertainty is  $\sigma_z \sim 0.004$ .<sup>2</sup>Redshift flag:

0 – flux is in small knots, so we do not measure an integrated flux for lines

1 – single line

1.5 – single line, inferred to be [OII], but with redshifted H $\beta$ , [OIII] falling in region of low sensitivity2 – single line, inferred to be [OII], but with redshifted H $\beta$ , [OIII] falling in region of good sensitivity

3 – single line with good reason to infer line (see text) 4 – multiple lines

<sup>3</sup>Photometry for the filterless direct image, given on the STMAG system.<sup>4</sup> SPS J030221.47+001150.6 is detected in the J030220.8+001153.9 field, while SPS J030210.18+001140.0 is detected in the J030210.9+001155.3 field.<sup>5</sup> SPS J095615.40+694535.3 is detected in the J095618.3+694537.0 field, while SPS J095628.10+694551.9 is detected in the J095623.8+694540.6 field.<sup>6</sup> This object is detected in both the J1213008+121420.7 and J1213013+121418.3 fields.

Table 4. Detected Objects

obj name	line	line flux <sup>1</sup>	$N_\sigma$	$W_{obs}$ (Å)	continuum $\sigma^2$
SPS J001716.56+160239.5	[OII]	1.35	3.7	141	0.5
SPS J010030.43-332823.4	[OII]	2.34	5.1	219	0.5
SPS J010329.80+131508.9	[OII]	4.74	10.5	156	1.5
	H $\delta$	0.250	2.1	7	2.9
	H $\gamma$	0.860	3.2	30	1.6
	H $\beta$	1.20	3.3	58	0.7
	[OIII]4959	5.94	8.0	240	0.8
	[OIII]5007	12.6	14.5	481	0.7
SPS J021048.23-393308.0	[OII]	2.54	4.1	110	0.7
	H $\beta$	1.21	-2	...	...
	[OIII]5007	1.48	-2	...	...
SPS J030221.47+001150.6	[OII]	1.36	3.4	103	0.6
SPS J030210.18+001140.0	[OII]	2.90	5.4	191	0.4
SPS J031357.20-550113.5	[OII]	1.59	5.0	95	1.0
SPS J032022.38+152854.1	[OII]	2.46	2.7	297	0.2
SPS J033146.65-274453.5	[OII]	2.26	3.9	110	0.7
SPS J035431.21-493924.0	[OII]	0.770	6.1	146	0.8
	H $\beta$	0.840	3.5	115	0.6
	[OIII]4959	0.910	3.7	96	0.7
	[OIII]5007	3.88	13.2	419	0.7
SPS J041420.84+041417.6	[OII]	3.27	3.7	315	0.3
SPS J045437.34-532514.1	H $\alpha$	2.62	3.9	173	0.5
SPS J082344.12+292351.3	H $\beta$	0.690	1.7	81	0.4
	[OIII]4959	1.04	4.0	121	0.5
	[OIII]5007	1.42	4.7	167	0.5
	H $\alpha$	1.12	4.6	221	0.4
SPS J082346.66+292323.3	[OII]	1.70	2.7	170	0.3
SPS J084837.09+444819.8	H $\gamma$	2.10	5.9	18	9.0
	H $\beta$	4.53	6.9	36	5.8
	[OIII]4959	4.30	7.0	34	5.5
	[OIII]5007	8.25	10.7	66	4.8
SPS J084837.63+444845.3	[OII]	1.16	4.1	127	0.8
	H $\beta$	1.07	-2	...	...
SPS J084840.29+444845.8	H $\gamma$	0.480	2.1	11	3.6
	H $\beta$	0.910	3.0	19	3.9
	[OIII]4959	0.100	0.7	2	4.7
	[OIII]5007	0.970	4.3	20	4.3
	H $\alpha$	1.48	4.3	25	2.9
	[NII]6583	0.360	1.3	6	2.8
SPS J084904.39+445308.5	H $\beta$	1.01	4.0	120	0.5
	[OIII]4959	0.610	2.4	71	0.5
	[OIII]5007	3.47	9.0	416	0.4
SPS J084916.65+445457.7	[OII]	4.96	4.1	1895	0.0
SPS J092829.86-050121.9	[OII]	0.860	3.3	74	1.0
	H $\beta$	1.03	-2	...	...
SPS J092830.13-050118.6	[OII]	1.67	3.0	77	0.9
SPS J093340.07+550951.3	[OII]	1.67	3.2	70	1.2
	H $\beta$	0.400	1.5	23	1.1

Table 4—Continued

obj name	line	line flux <sup>1</sup>	$N_\sigma$	$W_{obs}$ (Å)	continuum $\sigma^2$
	[OIII]4959	1.12	3.9	65	1.1
	[OIII]5007	2.80	7.9	163	0.9
SPS J094810.95+131142.6	[OII]	1.77	4.6	184	0.5
	H $\beta$	1.64	-2	...	...
	[OIII]5007	2.39	-2	...	...
SPS J095240.06+435834.9	H $\beta$	0.200	1.2	16	0.8
	[OIII]4959	0.240	0.8	17	0.9
	[OIII]5007	0.830	2.8	59	0.8
SPS J095615.40+694535.3	[OII]	2.86	4.1	256	0.5
	H $\beta$	2.53	-2	...	...
	[OIII]5007	2.54	-2	...	...
SPS J100051.56+250858.6	[OII]	2.63	4.3	87	1.1
SPS J100051.67+250853.0	[OII]	3.64	5.1	272	0.4
SPS J100052.03+250839.2	[OII]	2.85	4.6	390	0.3
SPS J102049.27+365226.3	[OII]	2.22	4.6	66	1.5
SPS J102429.80+471314.2	[OII]	1.57	4.0	273	0.3
SPS J103640.31-034708.1	[OII]	1.03	2.6	51	1.3
SPS J104643.01-001212.7	[OII]	2.58	4.0	136	0.7
SPS J105655.06-034322.8	[OII]	2.69	4.3	78	1.1
SPS J105700.03-034400.9	H $\beta$	0.600	-2	...	...
	[OIII]4959	0.850	2.8	36	1.3
	[OIII]5007	1.97	6.7	85	1.5
	H $\alpha$	1.91	2.3	123	0.5
SPS J105756.33-031415.7	[OII]	1.85	2.6	104	0.6
SPS J105705.12-034137.2	H $\gamma$	0.700	2.5	26	1.2
	H $\beta$	1.28	2.7	73	0.8
	[OIII]4959	2.58	3.9	147	0.7
	[OIII]5007	4.22	7.0	251	0.7
	H $\alpha$	4.19	3.2	550	0.2
SPS J105702.81-034158.3	H $\beta$	0.200	1.	21	0.4
	[OIII]4959	0.750	2.7	93	0.4
	[OIII]5007	2.45	7.0	297	0.4
SPS J105708.69-034310.8	H $\beta$	0.970	2.3	89	0.5
	[OIII]4959	1.30	3.1	116	0.5
	[OIII]5007	1.69	4.7	152	0.6
	H $\alpha$	3.17	3.8	105	0.8
SPS J105708.06-034320.1	[OII]	6.58	11.7	395	0.7
SPS J110137.18-121131.1	[OII]	4.23	4.8	188	0.8
	H $\beta$	1.40	-2	...	...
	[OIII]5007	1.47	-2	...	...
SPS J112057.83+232306.6	[OII]	1.32	3.4	91	0.8
SPS J113338.51+041031.8	[OII]	4.55	4.7	233	0.6
	H $\beta$	2.74	-2	...	...
	[OIII]5007	3.15	-2	...	...
SPS J113950.96+660350.4	[OII]	1.04	2.8	48	1.1
SPS J115616.05+550215.4	[OII]	1.79	2.9	67	0.7
SPS J120113.92-185633.2	[OII]	2.94	4.0	101	1.0
	H $\beta$	3.05	2.3	256	0.2

Table 4—Continued

obj name	line	line flux <sup>1</sup>	$N_\sigma$	$W_{obs}$ (Å)	continuum $\sigma^2$
	[OIII]4959	0.580	0.7	48	0.2
	[OIII]5007	4.60	2.4	396	0.1
SPS J120112.82-185622.5	[OII]	1.98	3.9	209	0.4
SPS J121716.05-031607.0	[OII]	3.01	3.0	236	0.2
SPS J121901.51+470804.6	[OII]	2.15	3.3	115	0.8
SPS J121904.77+470754.4	[OII]	1.54	4.5	105	0.8
SPS J122821.87+123625.3	[OII]	2.08	4.5	179	0.6
SPS J122821.28+123636.9	[OII]	1.87	4.4	146	0.8
SPS J123103.19+121422.6	[OII]	1.34	3.9	153	0.4
	H $\beta$	0.270	1.4	35	0.3
	[OIII]4959	0.930	0.8	119	0.2
	[OIII]5007	2.53	2.3	363	0.1
SPS J123108.68+121542.7	[OII]	1.48	4.2	115	0.8
	H $\beta$	1.55	-2	...	...
	[OIII]5007	2.32	-2	...	...
SPS J123348.78+023212.4	[OII]	3.02	3.5	307	0.3
	H $\beta$	2.79	-2	...	...
SPS J123410.44+023311.7	[OII]	1.56	4.8	190	0.4
SPS J123632.10+621758.3	[OII]	0.760	5.3	57	1.9
	H $\beta$	8.49	-2	...	...
SPS J123702.88+140744.9	H $\beta$	0.430	2.3	255	0.1
	[OIII]4959	0.870	2.6	645	0.1
	[OIII]5007	2.30	4.9	1787	0.1
SPS J123705.08+140801.3	H $\gamma$	0.800	4.0	44	1.7
	H $\beta$	1.24	5.9	81	1.5
	[OIII]4959	2.79	16.0	174	1.7
	[OIII]5007	8.71	41.5	538	1.5
	H $\alpha$	4.25	10.	160	1.3
SPS J123703.08+140803.7	[OII]	0.810	2.6	183	0.4
	H $\beta$	0.780	3.6	155	0.5
	[OIII]5007	1.45	-2	...	...
SPS J123704.59+140822.5	[OII]	1.04	3.4	56	1.5
SPS J125055.99+105042.5	[OII]	1.99	5.6	51	2.0
	H $\beta$	1.33	-2	...	...
	[OIII]5007	1.35	-2	...	...
SPS J125054.02+105101.1	[OII]	2.97	5.6	297	0.4
SPS J125917.75+362702.7	H $\beta$	0.670	2.0	21	1.7
	[OIII]4959	0.640	2.3	21	1.6
	[OIII]5007	2.12	5.0	75	1.5
	[OI]6300	1.13	1.8	95	0.3
	H $\alpha$	2.70	3.9	210	0.4
	[SII]	0.900	1.8	65	0.4
SPS J130002.95+275342.0	[OII]	0.880	3.2	214	0.3
	H $\beta$	1.04	-2	...	...
	[OIII]5007	1.04	2.3	50	0.8
SPS J130016.01+275405.5	[OII]	0.750	2.7	78	0.6
	H $\beta$	0.450	2.2	165	0.2
	[OIII]4959	0.660	2.0	290	0.1

Table 4—Continued

obj name	line	line flux <sup>1</sup>	$N_\sigma$	$W_{obs}$ (Å)	continuum $\sigma^2$
	[OIII]5007	2.18	3.4	1041	0.1
SPS J130927.26+292229.3	[OII]	0.220	0.9	11	0.9
	H $\beta$	1.25	1.8	25	1.2
	[OIII]4959	1.54	2.3	26	1.5
	[OIII]5007	2.28	4.1	39	1.7
SPS J131812.38-000507.4	H $\alpha$	7.00	6.1	85	1.9
	[SII]	2.21	3.3	39	1.5
SPS J131810.94-000444.1	[OII]	1.30	3.8	42	1.7
SPS J131810.43-000453.8	OII1302	5.98	30.0	35	20
	SiIV1398	5.70	40.0	35	20
	NIV]1486	1.35	28.0	9	20
	CIV1550	22.1	50.0	159	20
	CIII]1909	13.7	50.0	141	20
SPS J132511.10+301418.3	[OII]	1.23	3.4	105	0.7
SPS J133008.55+470741.8	[OII]	1.62	3.6	124	0.5
	H $\beta$	0.270	1.1	159	0.1
	[OIII]4959	0.230	0.8	79	0.1
	[OIII]5007	4.87	3.5	2341	0.0
SPS J133006.46+470719.4	[OII]	1.73	3.1	82	0.8
	H $\beta$	2.52	-2	...	...
SPS J134035.18+273417.1	H $\gamma$	0.340	1.3	41	0.5
	H $\beta$	1.03	3.5	82	0.8
	[OIII]4959	0.580	2.6	39	0.9
	[OIII]5007	2.57	9.3	175	1.0
SPS J134322.44+021542.7	[OII]	3.39	2.9	104	0.5
SPS J134606.52+015858.2	H $\beta$	1.18	1.9	99	0.3
	[OIII]4959	0.670	1.1	60	0.3
	[OIII]5007	5.21	5.0	489	0.3
SPS J134608.36+015922.6	[OII]	4.64	7.3	492	0.4
	H $\beta$	1.23	2.3	427	0.1
SPS J134721.93+021407.2	H $\gamma$	3.26	4.2	14	6.4
	H $\beta$	5.27	7.0	29	6.5
	[OIII]4959	2.63	3.4	15	6.4
	[OIII]5007	3.13	5.1	17	6.9
	H $\alpha$	34.3	22.3	262	2.5
SPS J134721.97+021405.7	[OIII]5007	1.97	3.7	210	0.4
SPS J140140.40+150857.3	[OII]	3.58	3.6	122	0.9
	H $\beta$	1.56	-2	...	...
	[OIII]5007	1.63	-2	...	...
SPS J141824.25+523420.0	[OII]	1.32	3.7	61	1.4
SPS J142427.43+225959.8	[OII]	1.47	4.2	102	0.8
SPS J142957.15+420713.1	[OII]	2.48	4.4	77	1.7
	H $\beta$	0.710	-2	...	...
	[OIII]4959	0.930	2.5	31	1.6
	[OIII]5007	2.81	7.1	89	1.6
SPS J142955.57+420714.3	[OII]	1.62	4.5	89	1.0
SPS J142956.79+420729.4	[OII]	1.66	5.5	259	0.4
	H $\beta$	0.440	-2	...	...

Table 4—Continued

obj name	line	line flux <sup>1</sup>	$N_\sigma$	$W_{obs}$ (Å)	continuum $\sigma^2$
	[OIII]5007	0.520	-2	...	...
SPS J144449.32+384521.1	H $\alpha$	3.06	4.2	30	2.9
SPS J151617.05-001337.9	[OII]	3.27	5.3	126	0.9
SPS J155003.49+212318.9	[OII]	1.87	2.6	123	0.5
SPS J160956.65+653334.6	H $\beta$	0.680	20.0	5	3
	[OIII]4959	4.65	50.0	31	3
	[OIII]5007	10.6	50.0	69	3
	[FeVII]	1.15	50.0	7	5
	[OI]	0.350	25.0	2	5
	H $\alpha$	15.8	50.0	87	1
	[SII]	2.58	50.0	14	6
SPS J162357.69+262830.2	H $\beta$	0.790	5.0	21	1
	[OIII]4959	0.690	4.5	17	0.9
	[OIII]5007	2.40	12.0	54	7.4
	[FeVII]5721	0.540	8.0	13	8
	H $\alpha$	2.20	20.0	66	3
	HeI7065	0.800	8.0	32	16
SPS J162354.88+262803.5	[OII]	4.67	8.0	279	5
SPS J162341.40+263433.0	H $\beta$	2.49	-2	...	...
	[OIII]5007	2.41	-2	...	...
	H $\alpha$	5.17	2.3	161	0.4
SPS J162444.27+234041.6	[OII]	4.18	3.7	374	0.3
SPS J164435.47+234221.2	H $\beta$	0.220	0.3	27	0.1
	[OIII]4959	2.06	2.7	280	0.2
	[OIII]5007	4.69	4.4	600	0.1
	H $\alpha$	2.07	2.8	254	0.2
SPS J164434.54+234207.9	[OII]	1.28	2.5	383	0.1
	H $\beta$	3.44	-2	...	...
	[OIII]5007	4.47	-2	...	...
SPS J164908.74+601414.5	[OII]	3.32	5.2	402	0.3
SPS J164909.64+601416.3	[OII]	2.19	4.3	122	0.8
SPS J204756.29-194709.4	H $\beta$	0.490	1.8	6	5.1
	[OIII]4959	1.74	4.6	22	4.7
	[OIII]5007	4.84	12.5	61	4.6
	[OI]6300	1.20	1.9	20	2.0
	H $\alpha$	9.44	7.9	158	1.5
SPS J204757.09-194653.3	H $\beta$	0.890	2.9	21	2.6
	[OIII]4959	1.32	4.2	29	2.9
	[OIII]5007	4.80	15.5	106	2.9
	H $\alpha$	5.35	4.5	130	1.1
SPS J224024.66-054723.3	[OII]	0.970	2.6	112	0.5
	H $\beta$	1.62	3.7	380	0.2
	[OIII]4959	1.52	3.7	325	0.2
	[OIII]5007	5.79	9.4	1250	0.1
SPS J224024.68-054744.5	[OII]	2.11	3.9	208	0.4
SPS J232435.91+280401.8	H $\alpha$	1.97	2.5	110	0.5
SPS J235036.79+271021.1	[OII]	2.29	3.1	116	0.5
SPS J235036.70+271024.2	[OII]	2.48	2.7	84	0.6

Table 4—Continued

obj name	line	line flux <sup>1</sup>	$N_\sigma$	$W_{obs}$ (Å)	continuum $\sigma^2$
SPS J235038.34+271003.2	[OII]	1.74	2.9	172	0.4
	H $\beta$	0.950	-2	...	...
	[OIII]5007	1.01	-2	...	...
SPS J235158.16+243036.2	[OII]	1.31	2.6	77	0.7
	H $\gamma$	0.680	2.7	49	1.0
	H $\beta$	0.490	2.6	41	0.9
	[OIII]4959	0.600	2.7	53	1.0
	[OIII]5007	1.68	7.5	148	1.0

<sup>1</sup>( $10^{-16}$  erg cm<sup>-2</sup> s<sup>-1</sup>)

<sup>2</sup>Continuum signal to noise ratio in a two pixel resolution element.

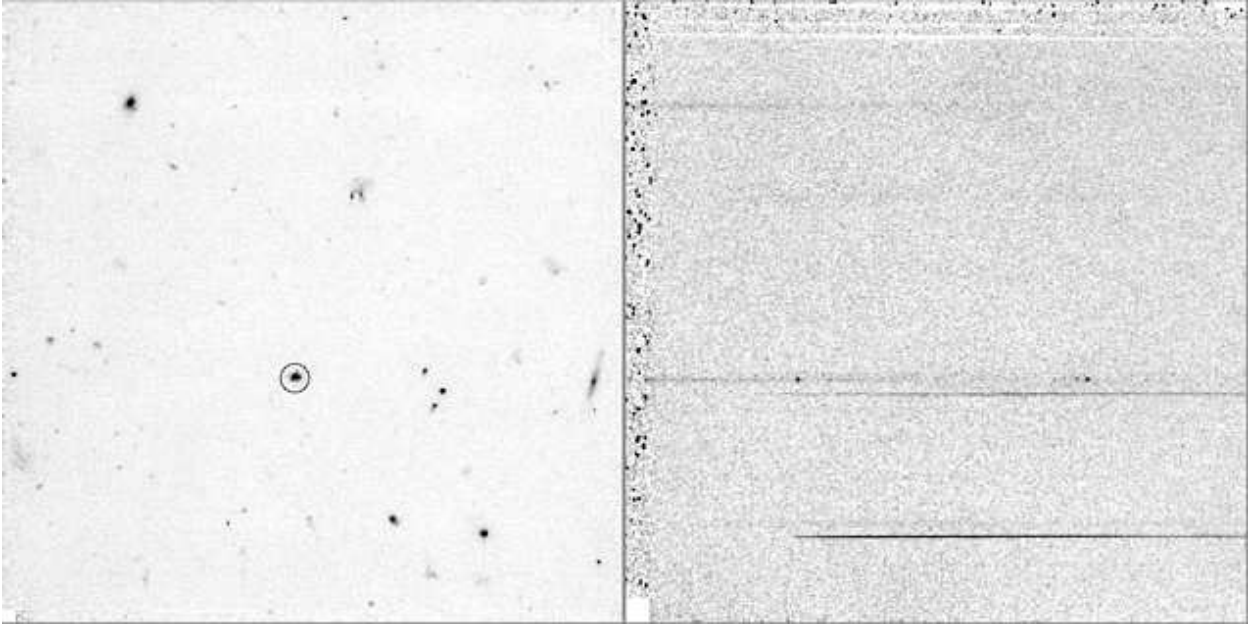


Fig. 1.— An image/spectrum pair of the J010329+131515 field from the deep SPS, containing one of the highest signal-to-noise ratio emission line objects (circled in the direct image); [OII], the [OIII] doublet, and  $H\beta$  are clearly visible in the 2 dimensional spectrum. The poor cosmic ray rejection is visible in the non-overlap regions resulting from telescope offsets.

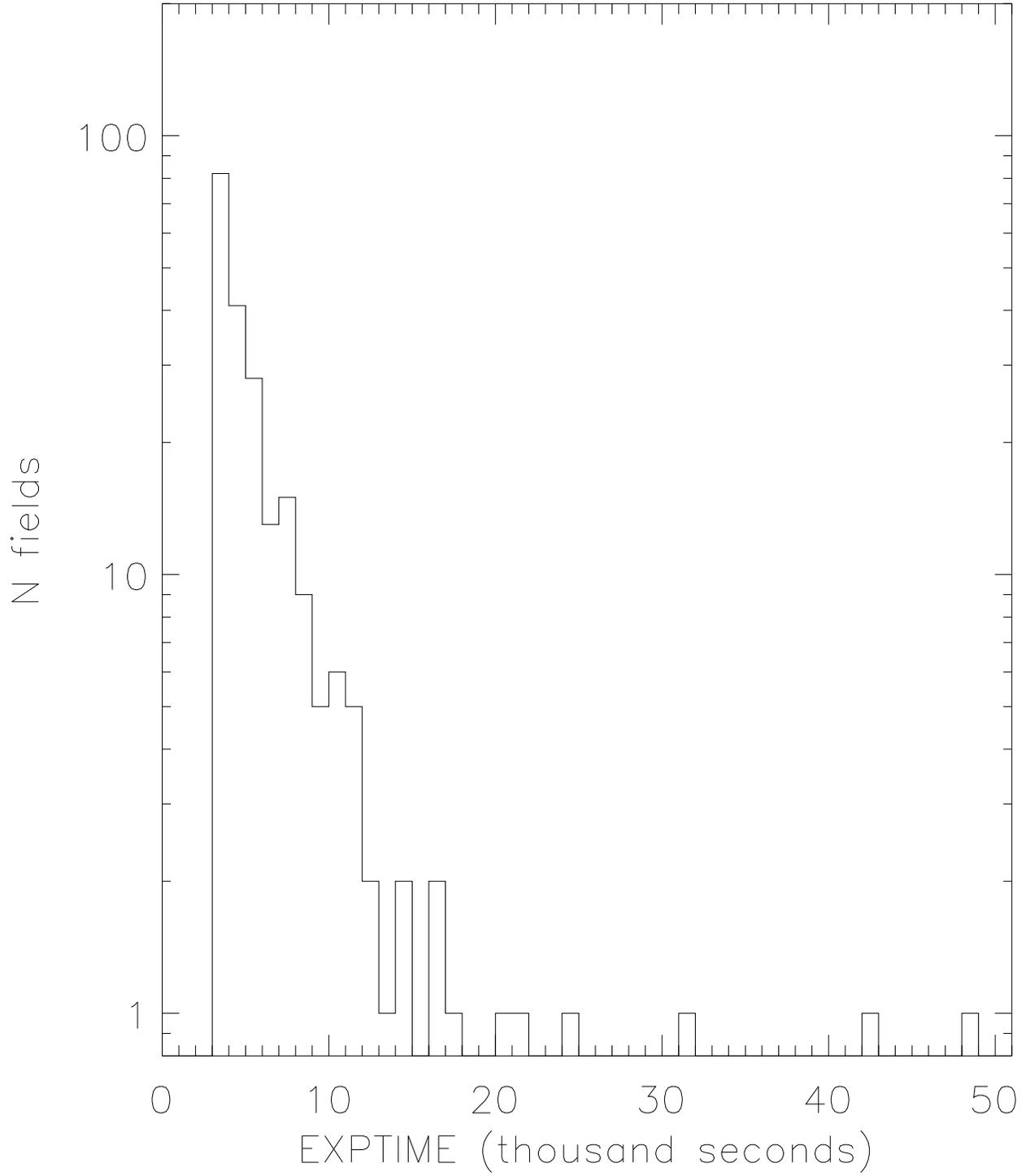
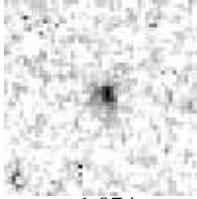
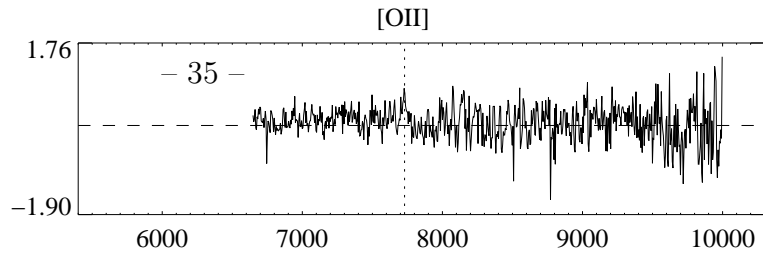


Fig. 2.— The distribution of exposure times in the deep SPS fields meeting the selection criteria (see text)

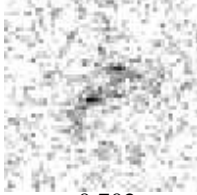
SPS J001716.56+160239.5



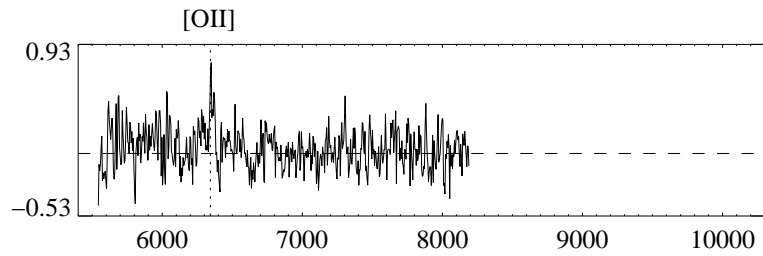
$z=1.074$



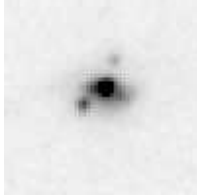
SPS J010030.43-332823.4



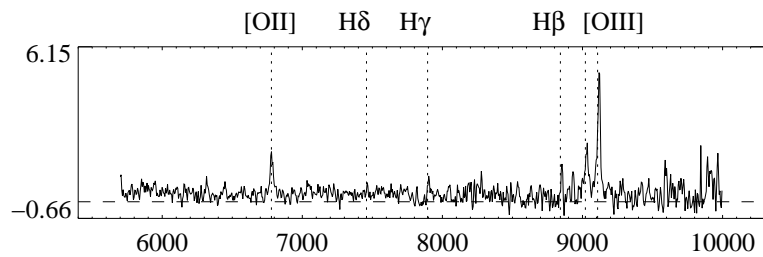
$z=0.702$



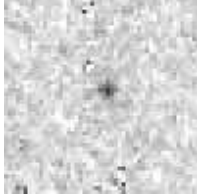
SPS J010329.80+131508.9



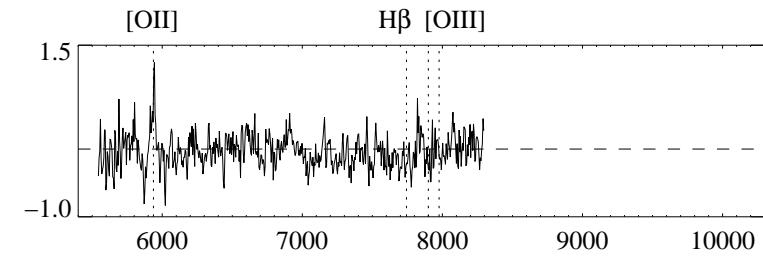
$z=0.819$



SPS J021048.23-393308.0



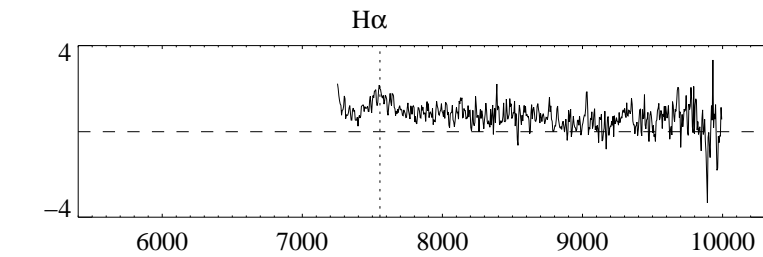
$z=0.593$



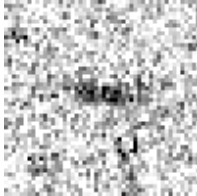
SPS J022828.08-011434.0



$z=0.151$



SPS J030221.47+001150.6



$z=0.920$

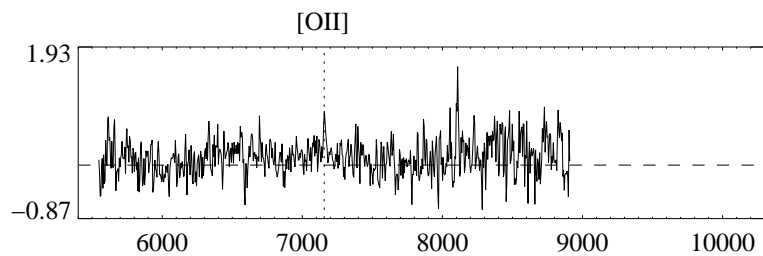


Fig. 3.— The direct image and extracted spectrum for SPS emission line objects. The postage stamp images are  $2.5''$  on each side, with the orientation of the original data. The postage stamp is centered on the region of strongest line emission, which may not coincide with the center of the object. The position of the  $H\alpha$ ,  $H\beta$ ,  $[OIII]$ , and  $[OII]$  emission lines are indicated by dotted lines in each spectrum whether they are detected or not. The wavelength of other emission lines is indicated if they are measured and presented in Table 3.

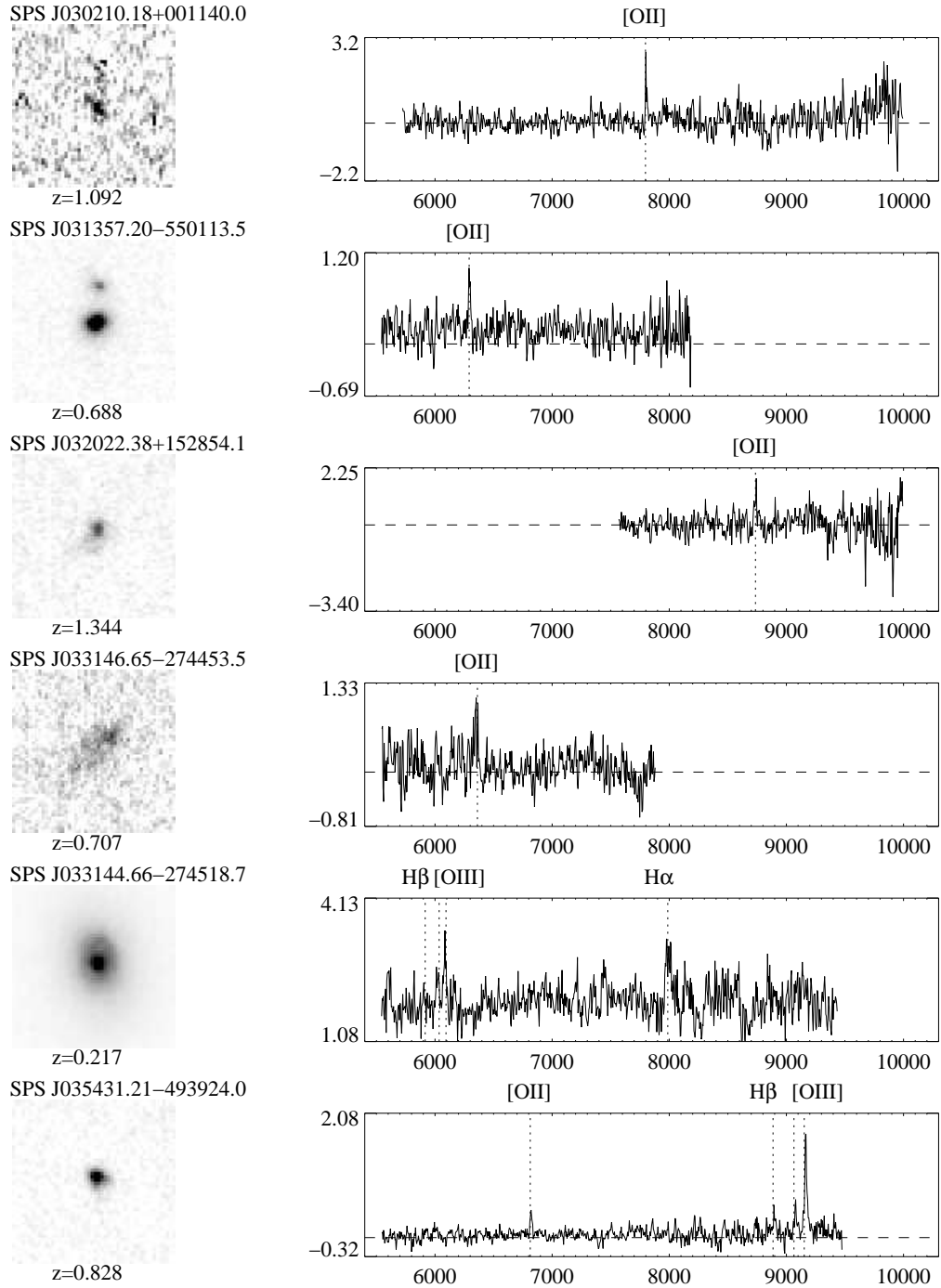


Fig. 4.— The direct image and extracted spectrum for SPS emission line objects, as in Figure 3.

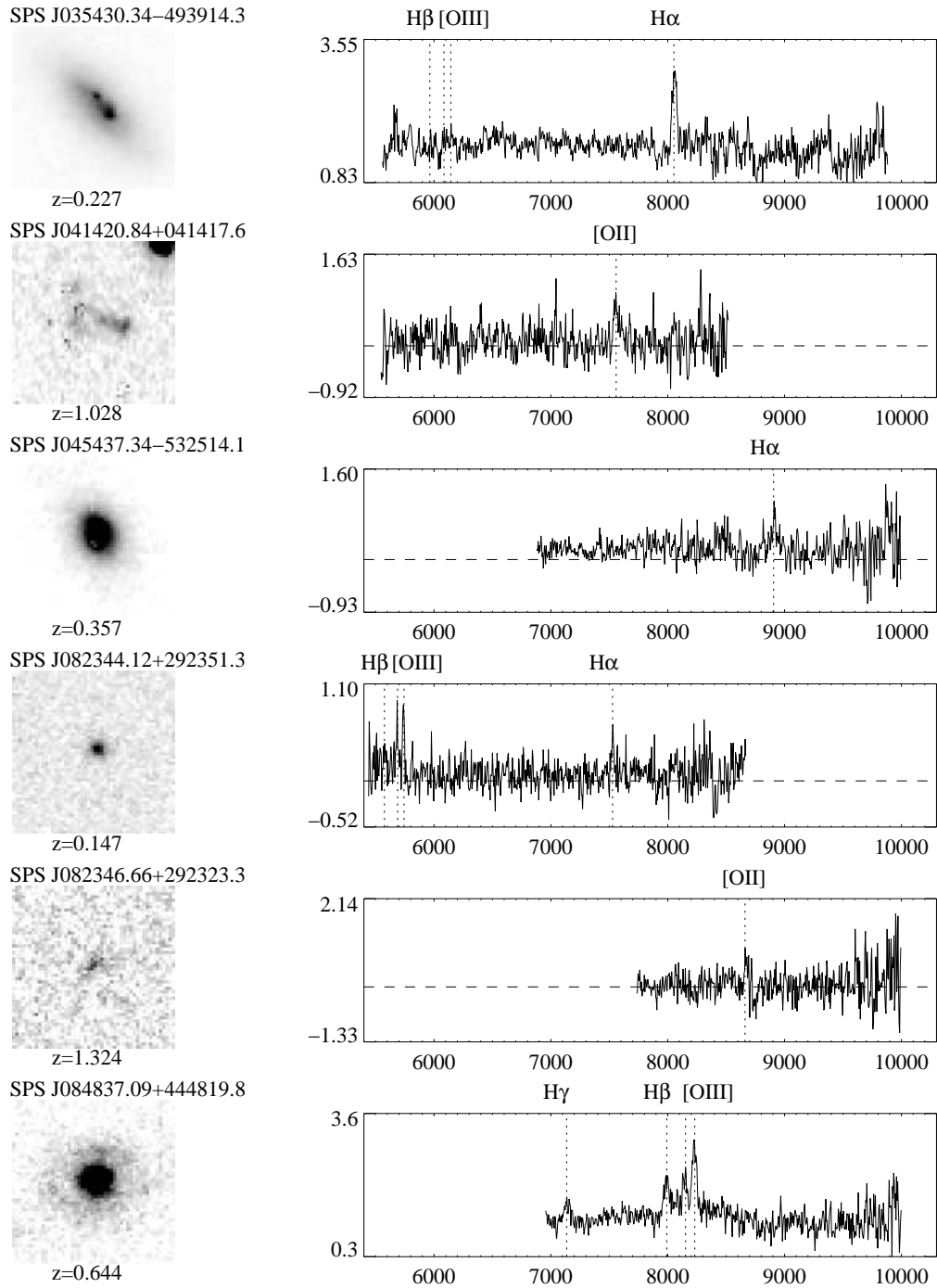


Fig. 5.— The direct image and extracted spectrum for SPS emission line objects, as in Figure 3.

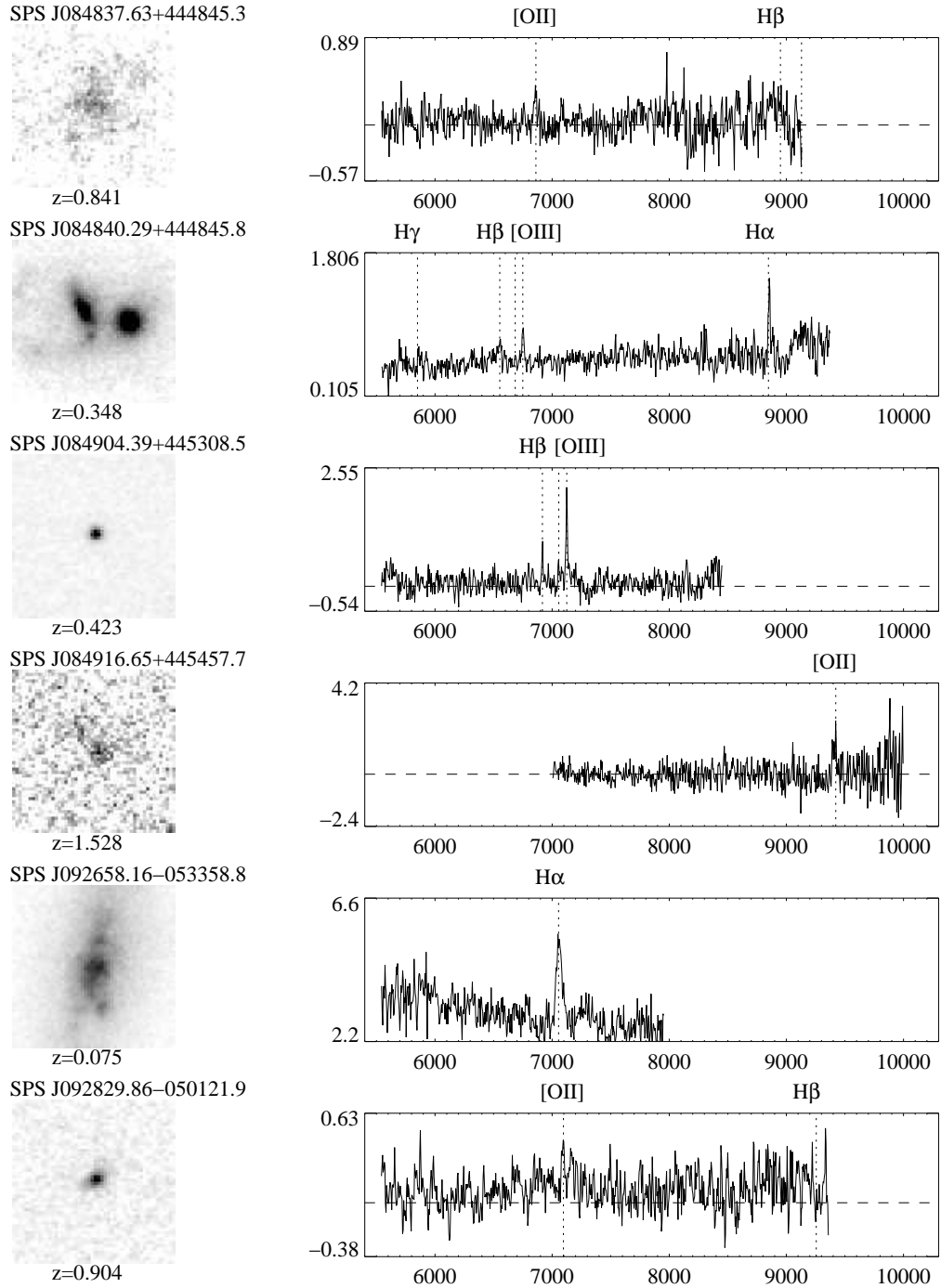


Fig. 6.— The direct image and extracted spectrum for SPS emission line objects, as in Figure 3.

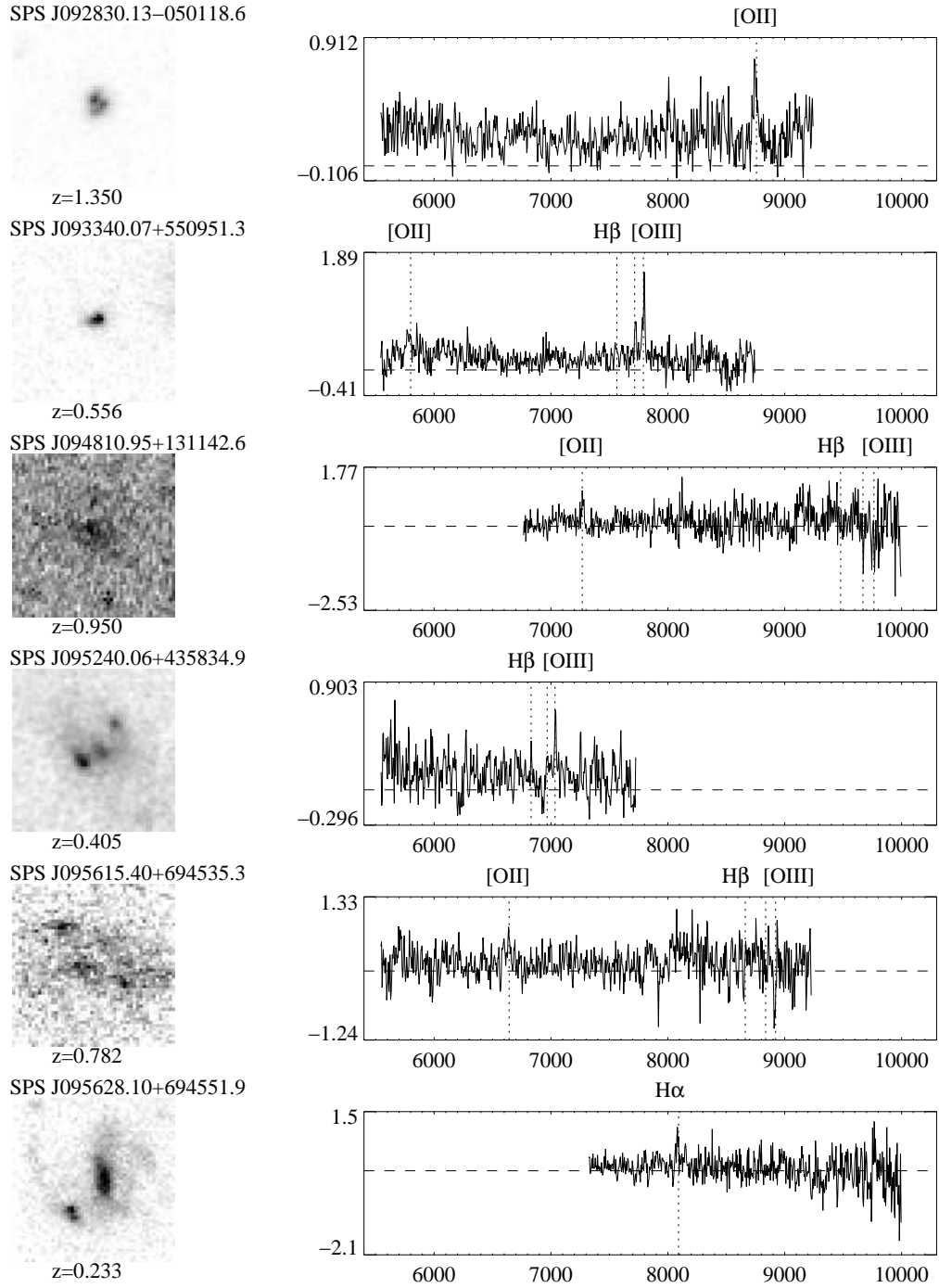


Fig. 7.— The direct image and extracted spectrum for SPS emission line objects, as in Figure 3.

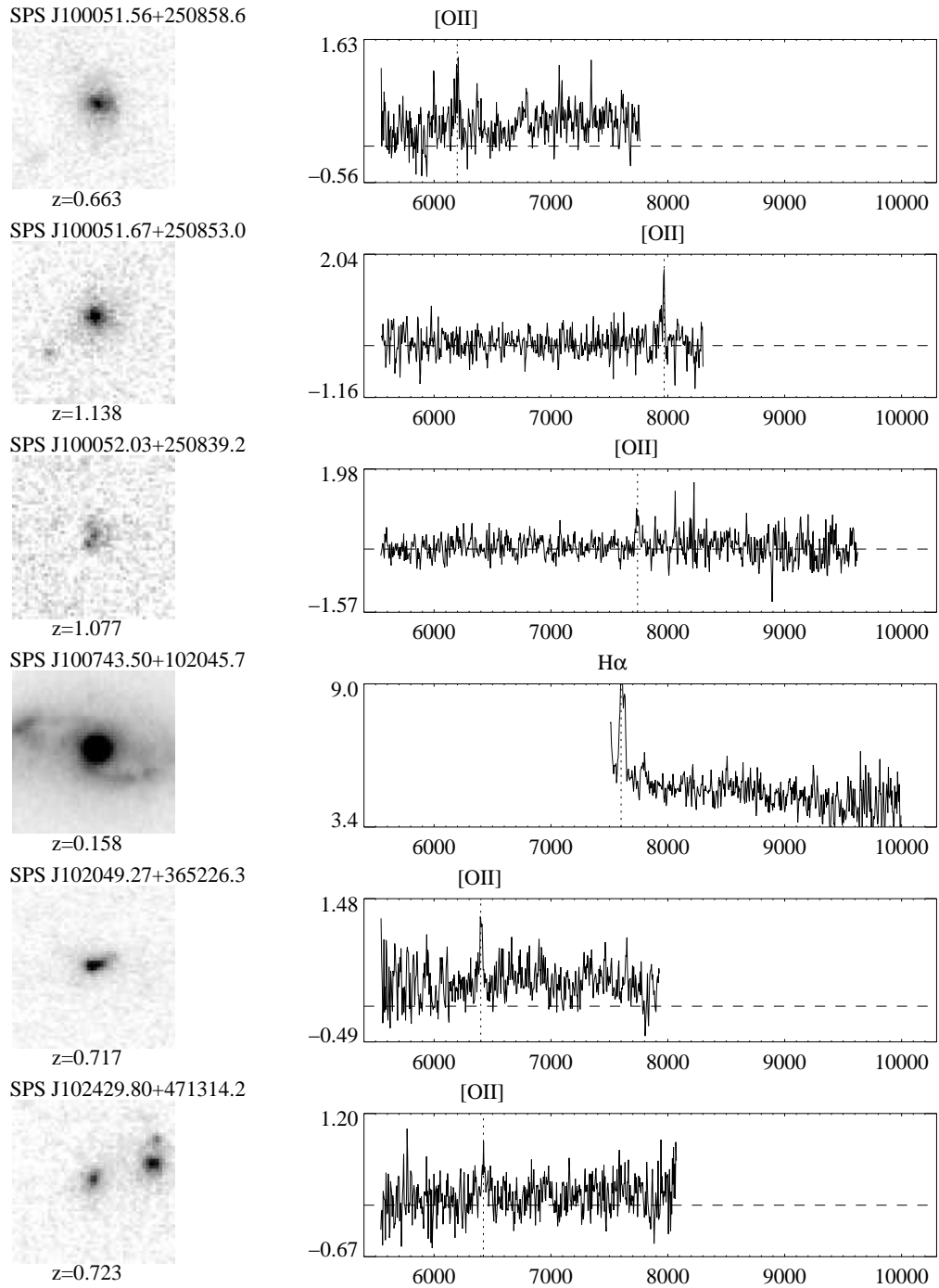


Fig. 8.— The direct image and extracted spectrum for SPS emission line objects, as in Figure 3.

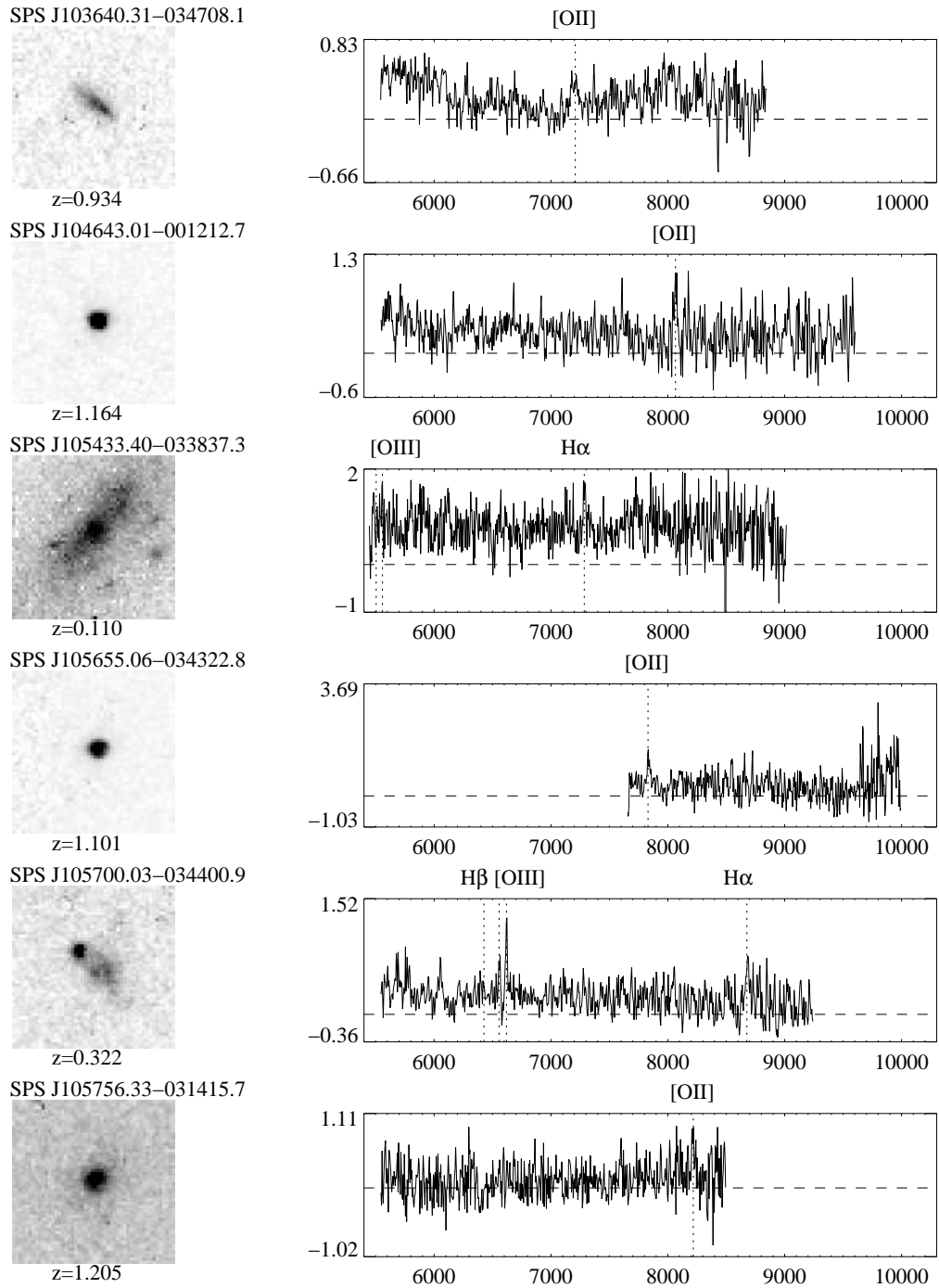


Fig. 9.— The direct image and extracted spectrum for SPS emission line objects, as in Figure 3.

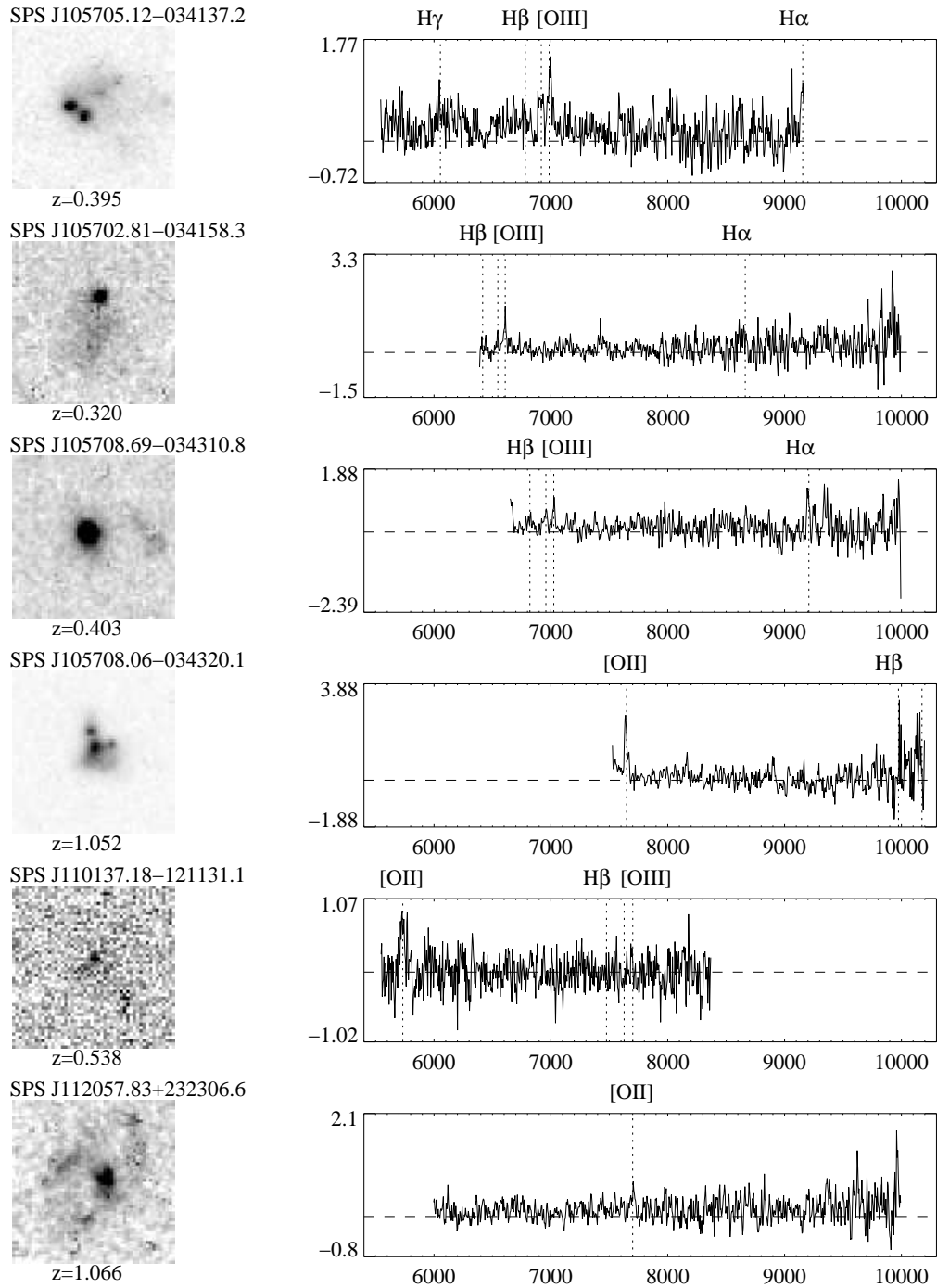


Fig. 10.— The direct image and extracted spectrum for SPS emission line objects, as in Figure 3.

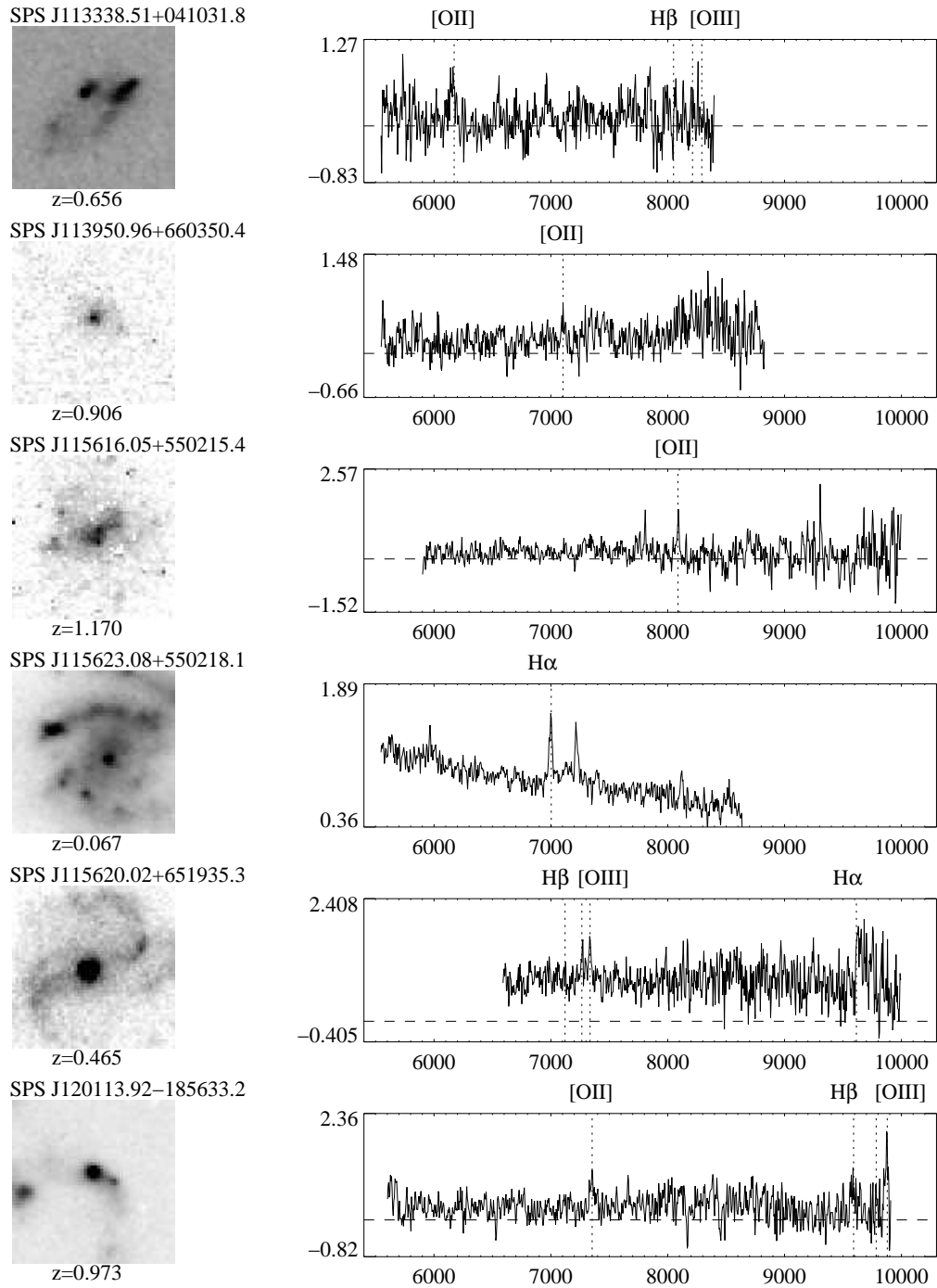


Fig. 11.— The direct image and extracted spectrum for SPS emission line objects, as in Figure 3.

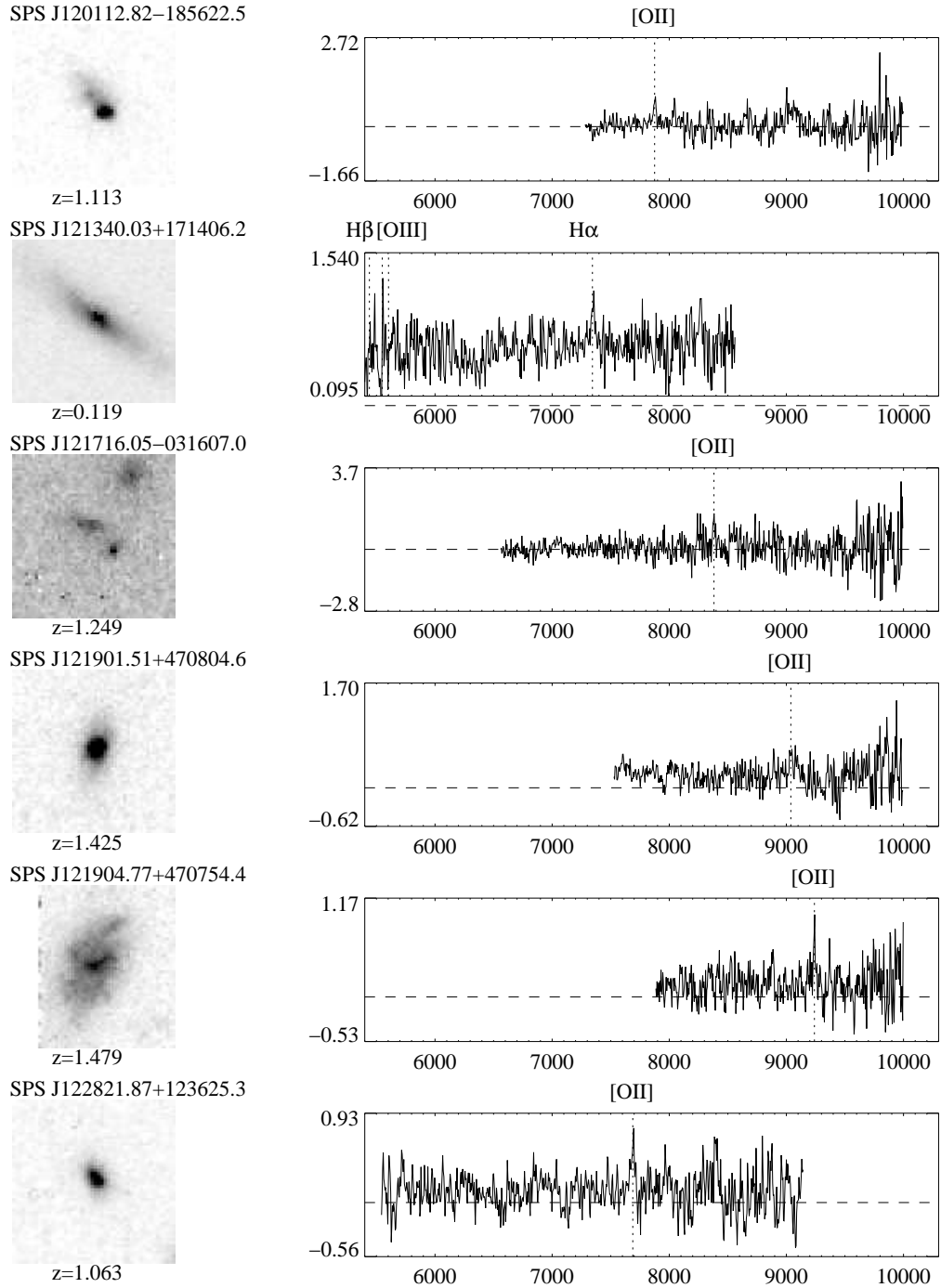


Fig. 12.— The direct image and extracted spectrum for SPS emission line objects, as in Figure 3.

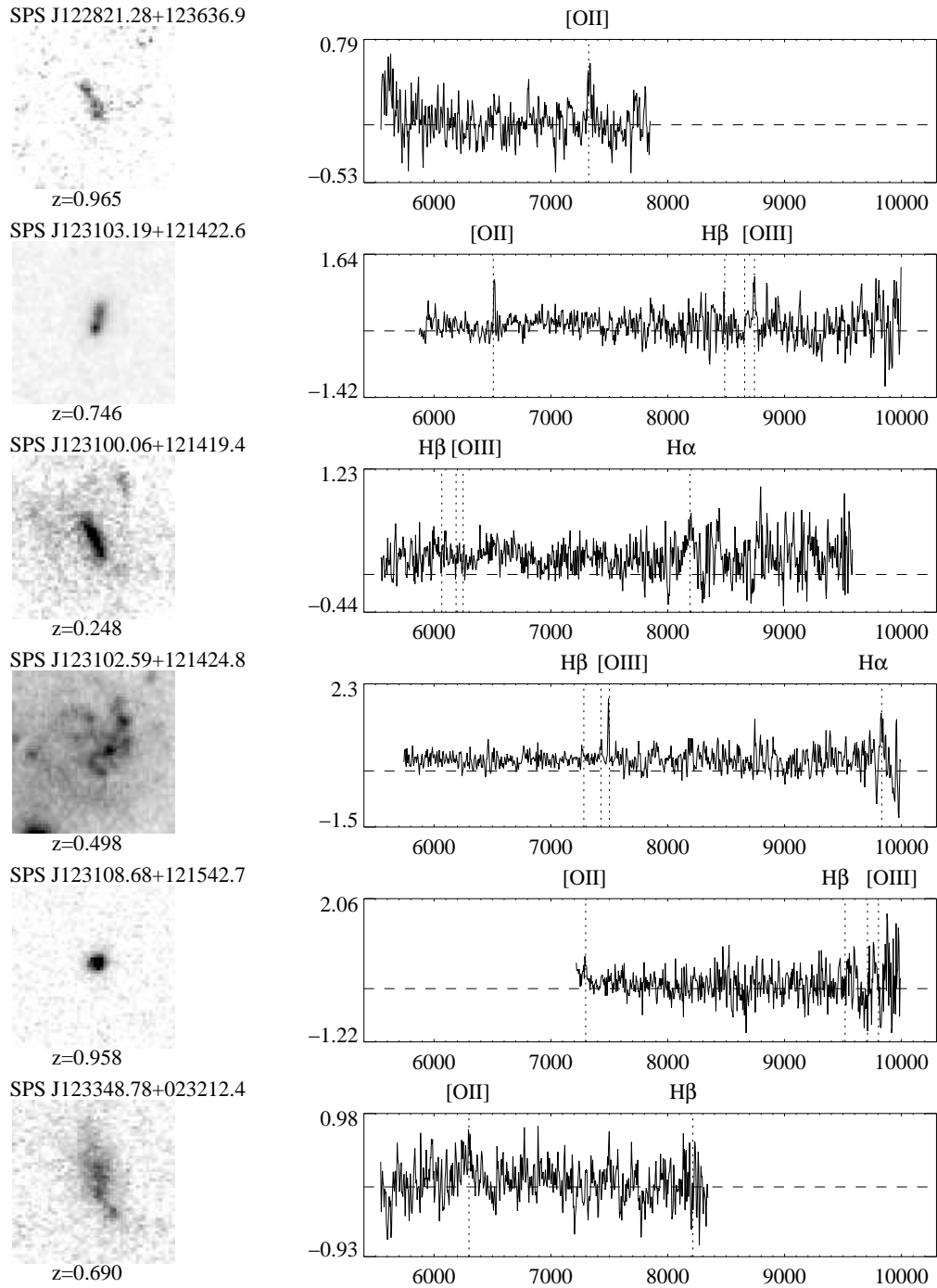


Fig. 13.— The direct image and extracted spectrum for SPS emission line objects, as in Figure 3.

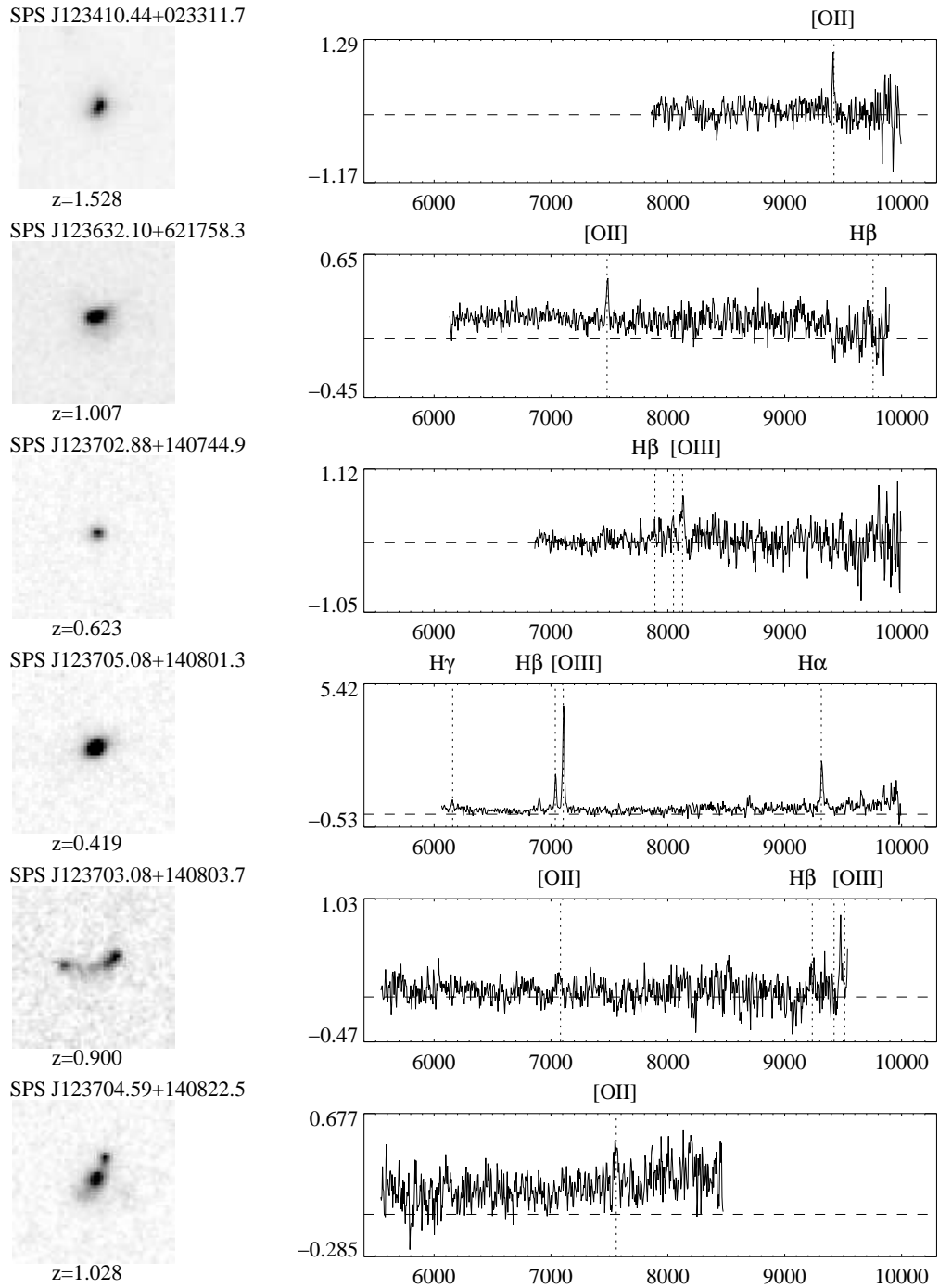


Fig. 14.— The direct image and extracted spectrum for SPS emission line objects, as in Figure 3.

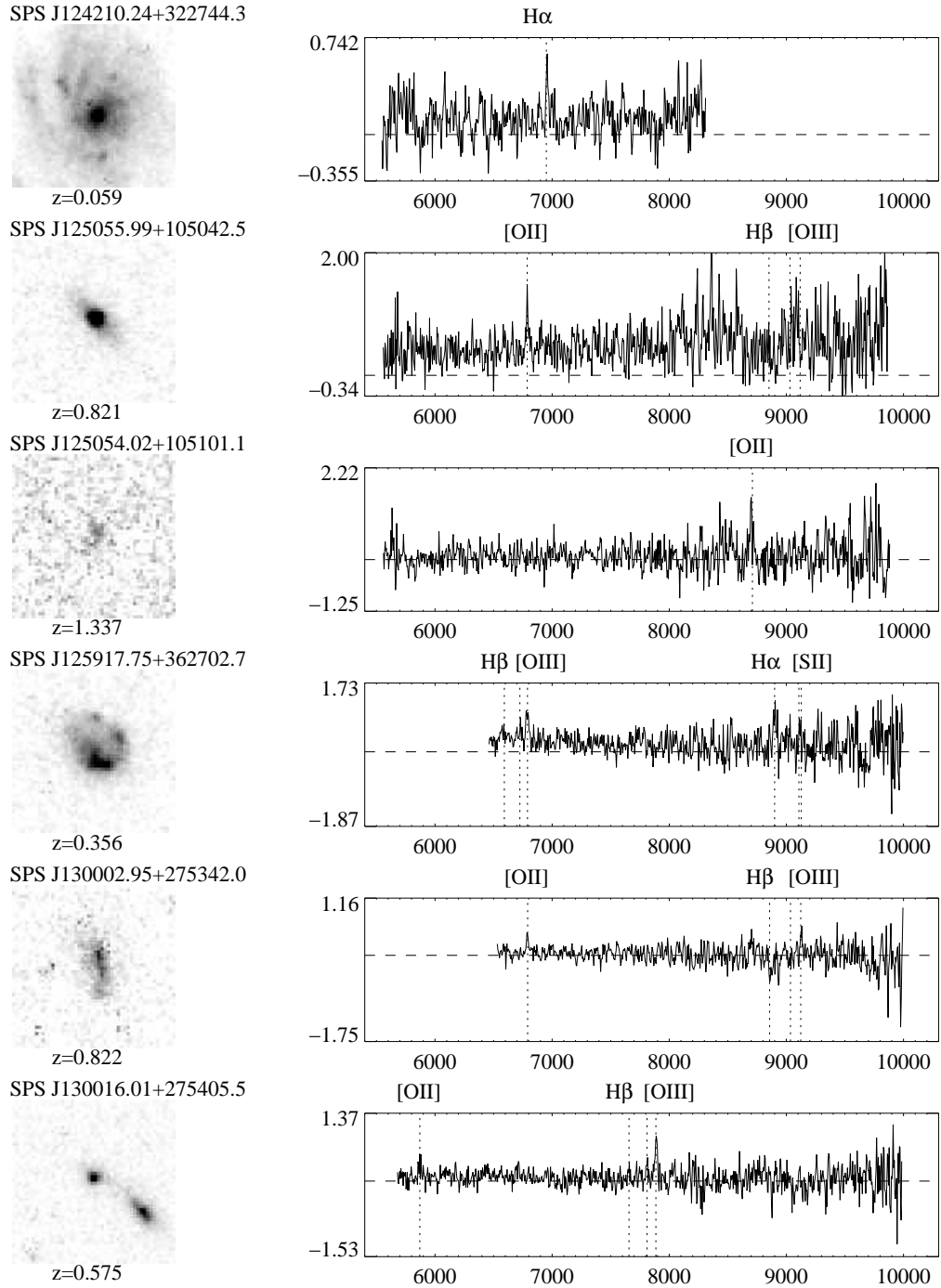


Fig. 15.— The direct image and extracted spectrum for SPS emission line objects, as in Figure 3.

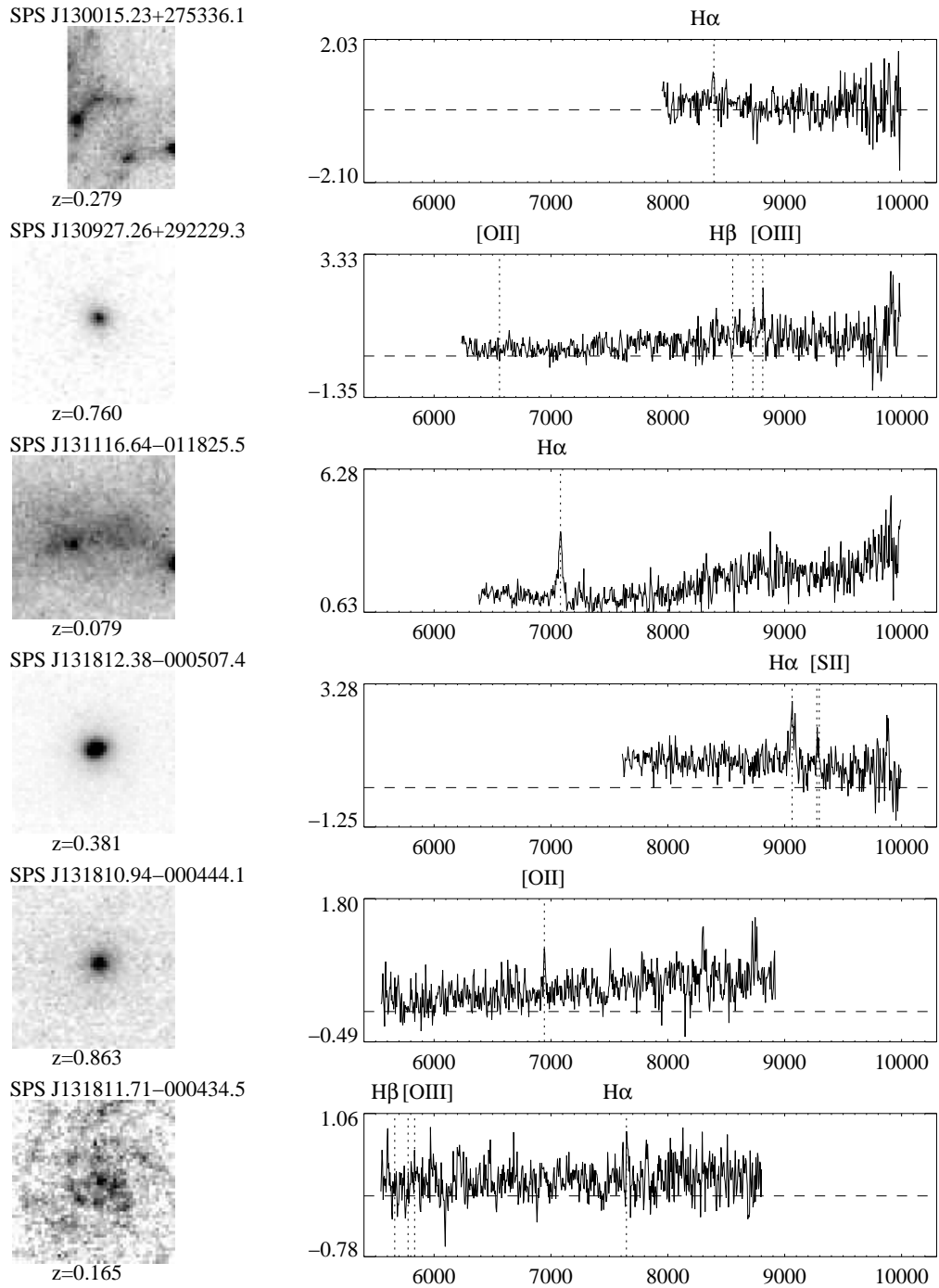


Fig. 16.— The direct image and extracted spectrum for SPS emission line objects, as in Figure 3.

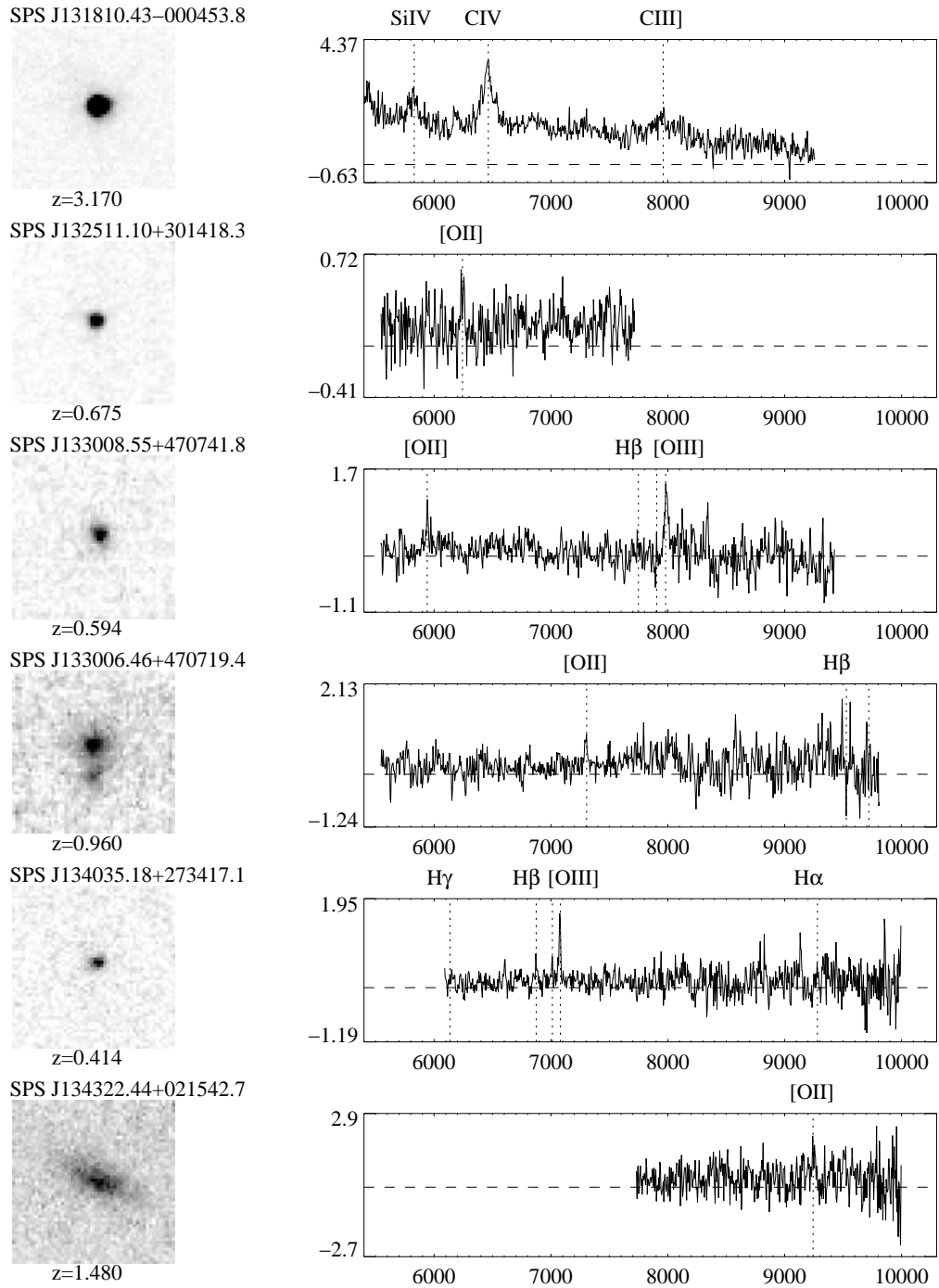


Fig. 17.— The direct image and extracted spectrum for SPS emission line objects, as in Figure 3.

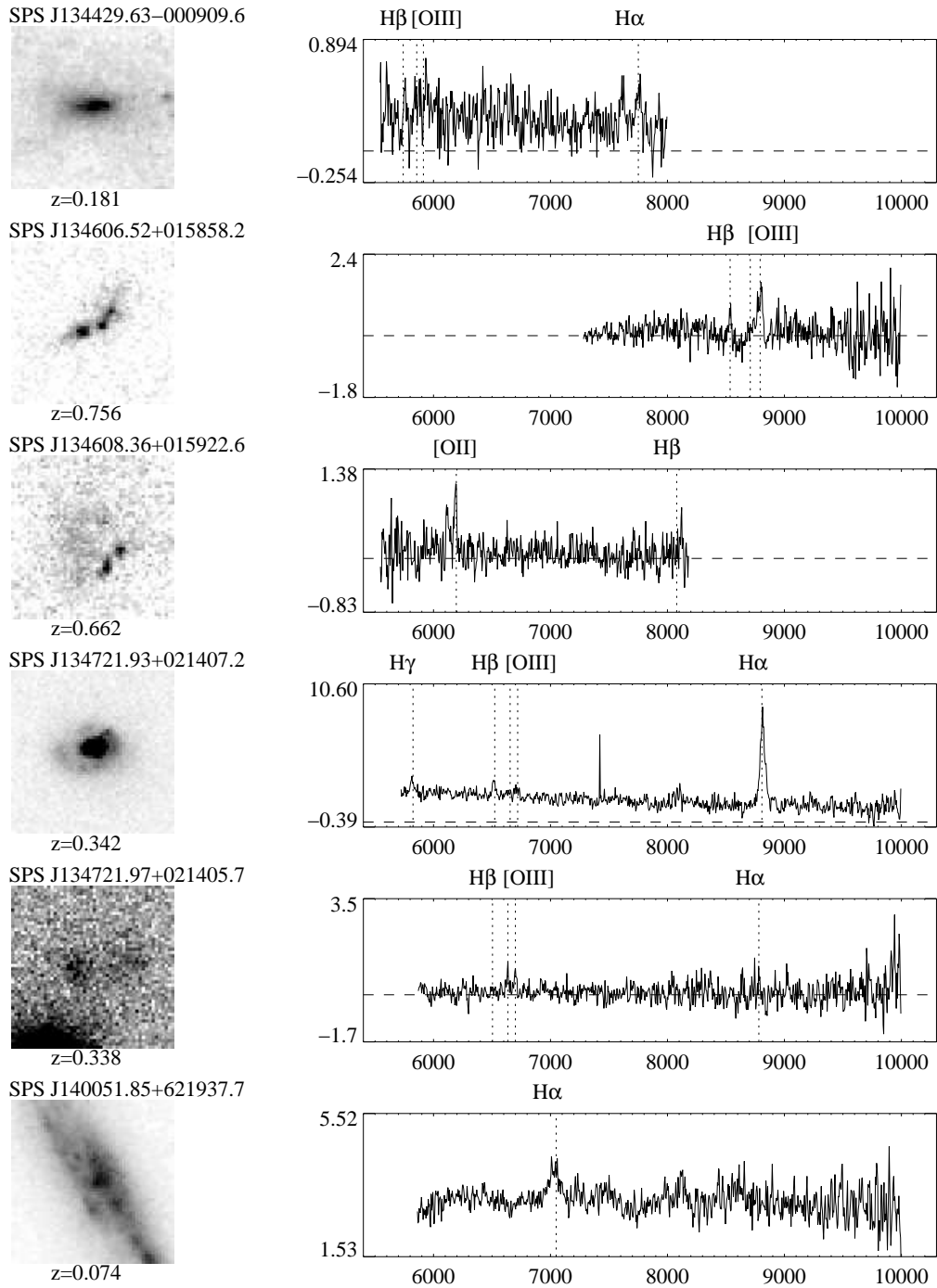


Fig. 18.— The direct image and extracted spectrum for SPS emission line objects, as in Figure 3.

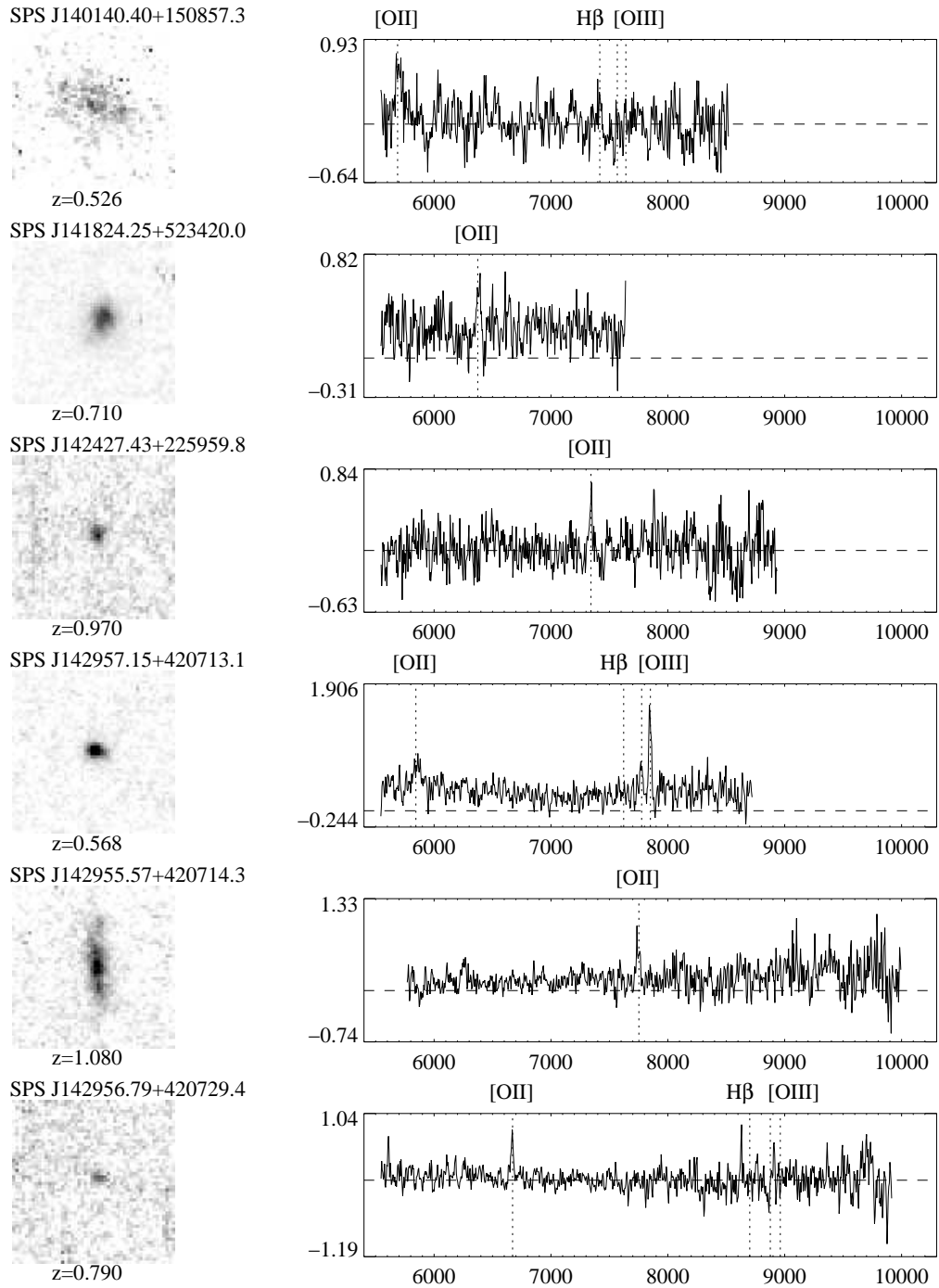


Fig. 19.— The direct image and extracted spectrum for SPS emission line objects, as in Figure 3.

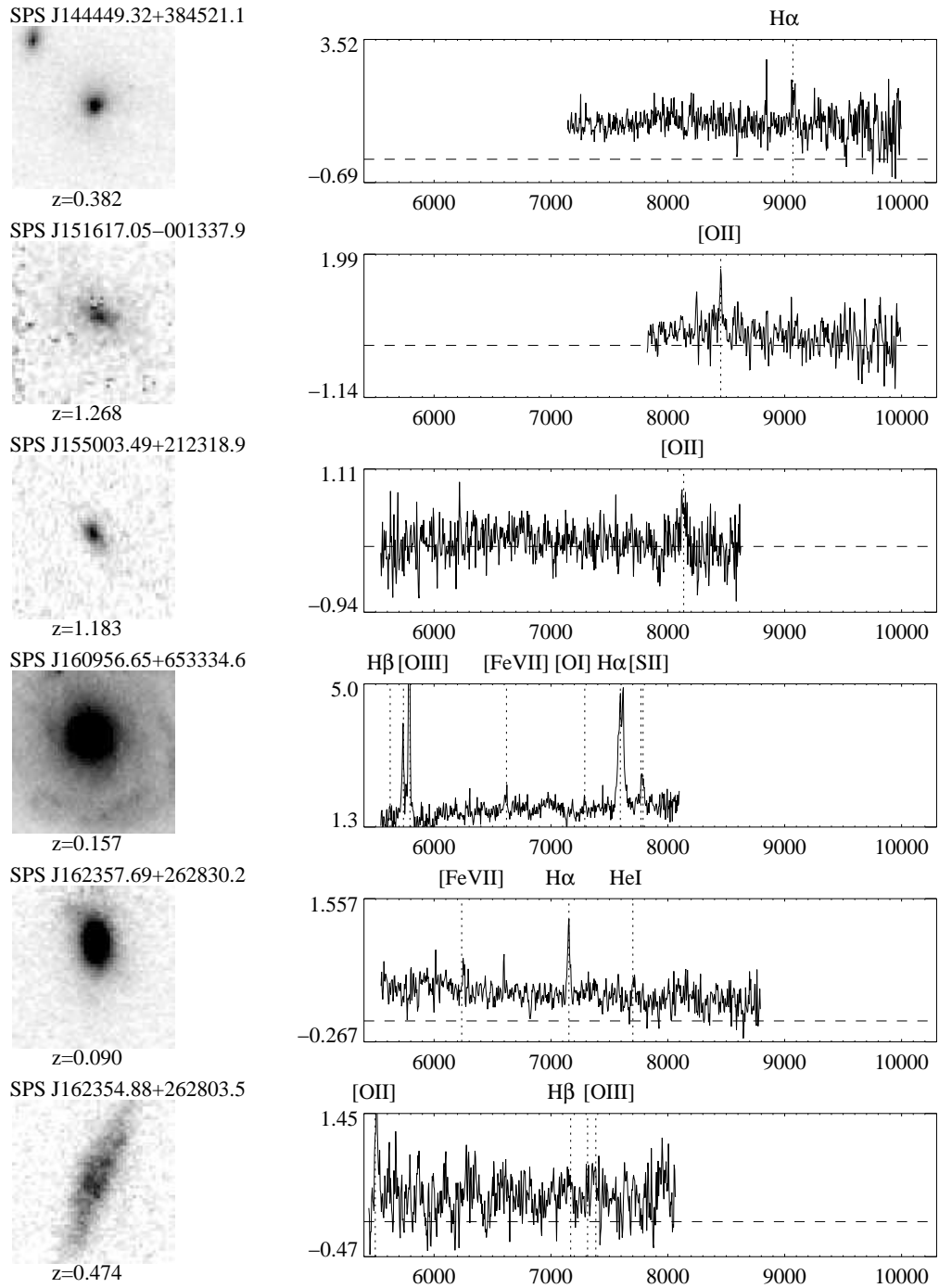


Fig. 20.— The direct image and extracted spectrum for SPS emission line objects, as in Figure 3.

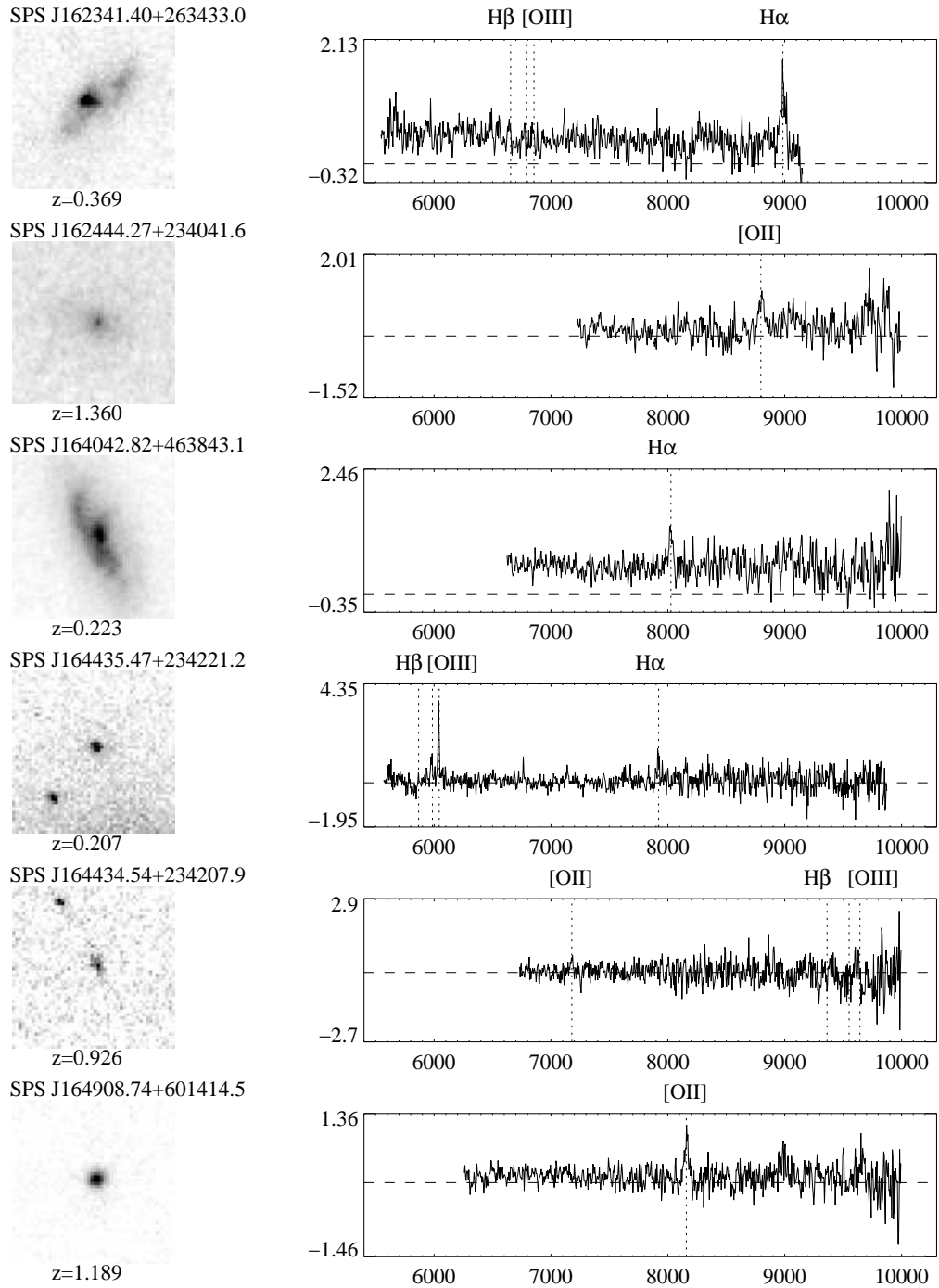


Fig. 21.— The direct image and extracted spectrum for SPS emission line objects, as in Figure 3.

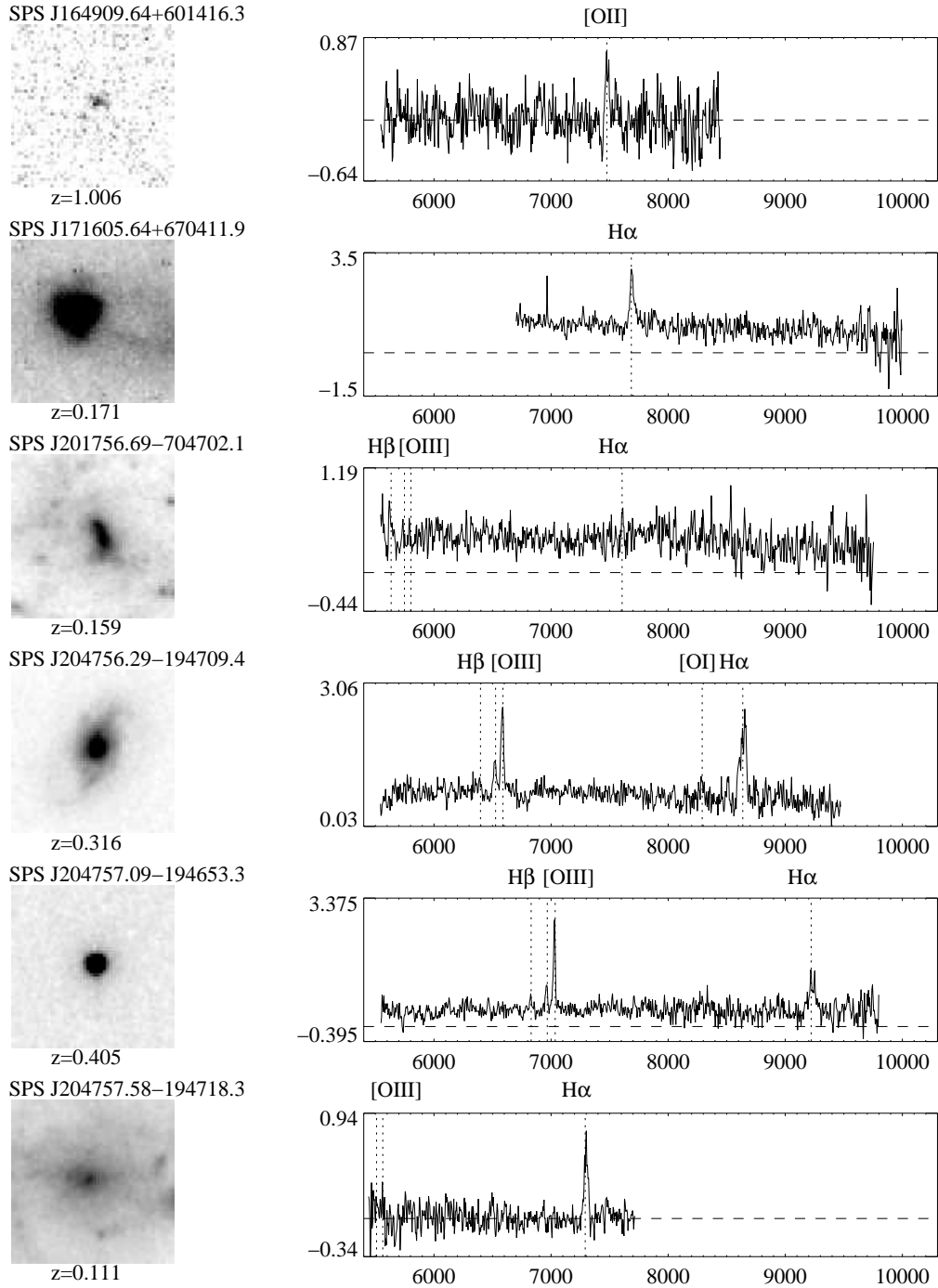


Fig. 22.— The direct image and extracted spectrum for SPS emission line objects, as in Figure 3.

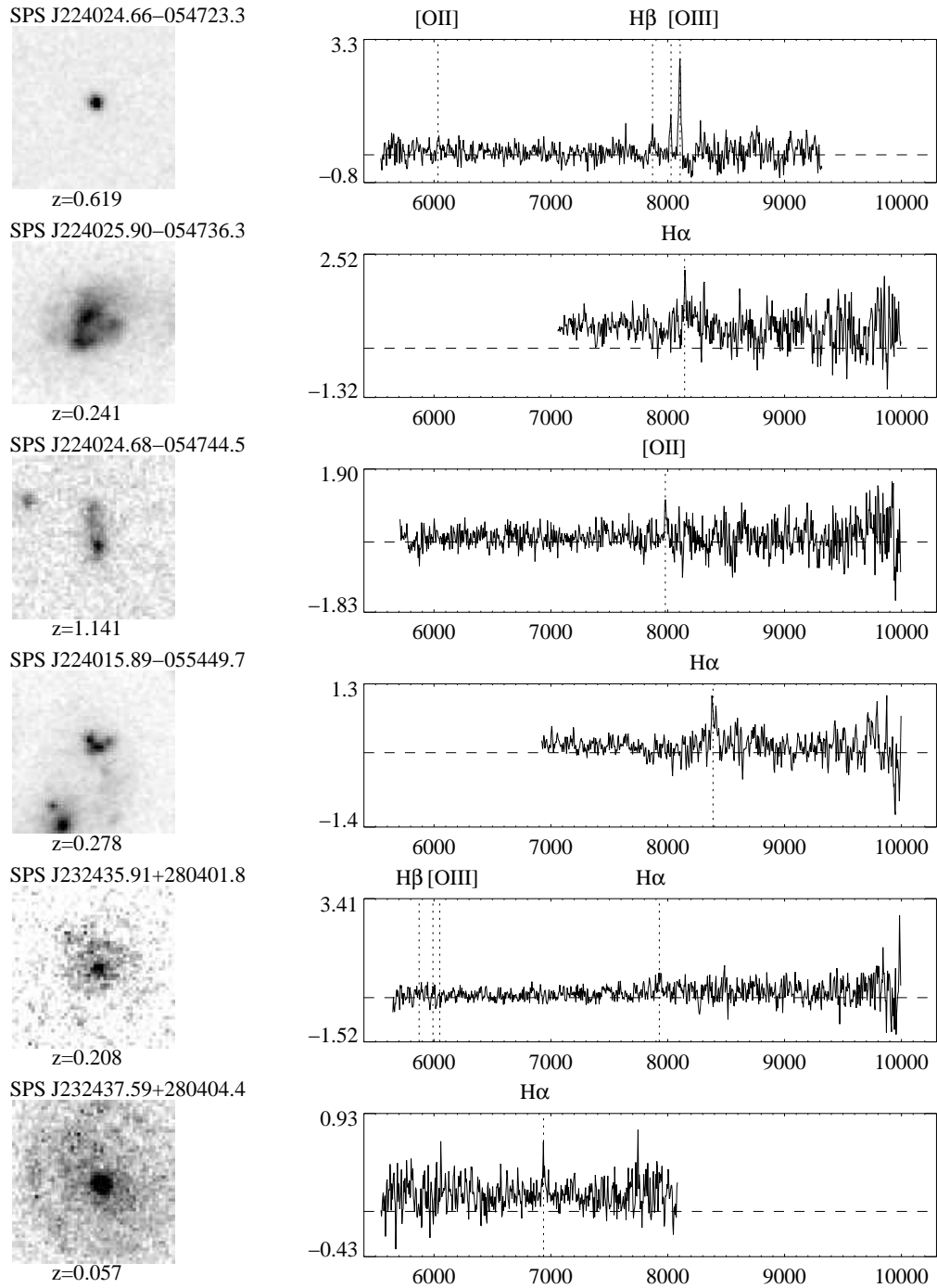


Fig. 23.— The direct image and extracted spectrum for SPS emission line objects, as in Figure 3.

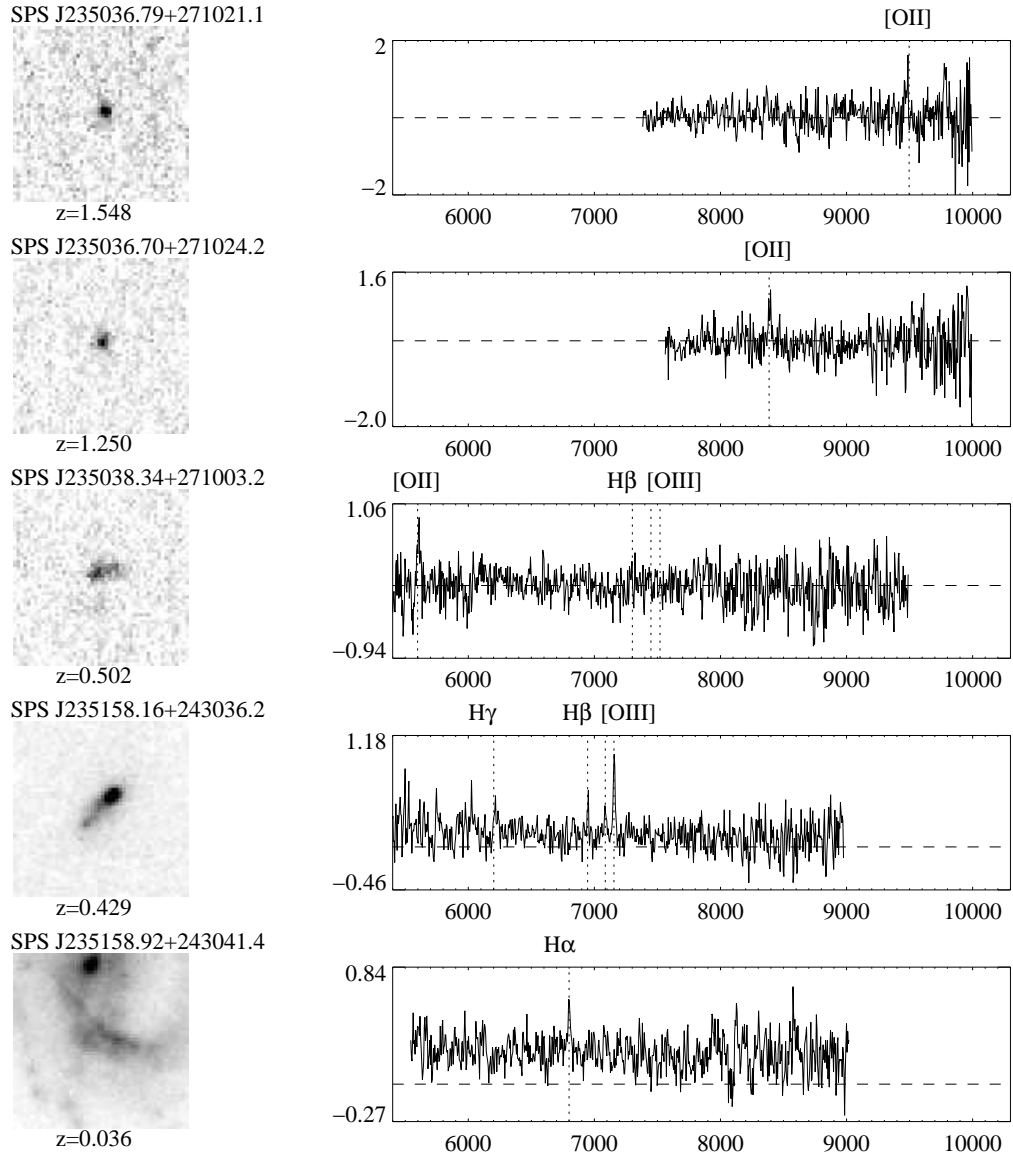


Fig. 24.— The direct image and extracted spectrum for SPS emission line objects, as in Figure 3.

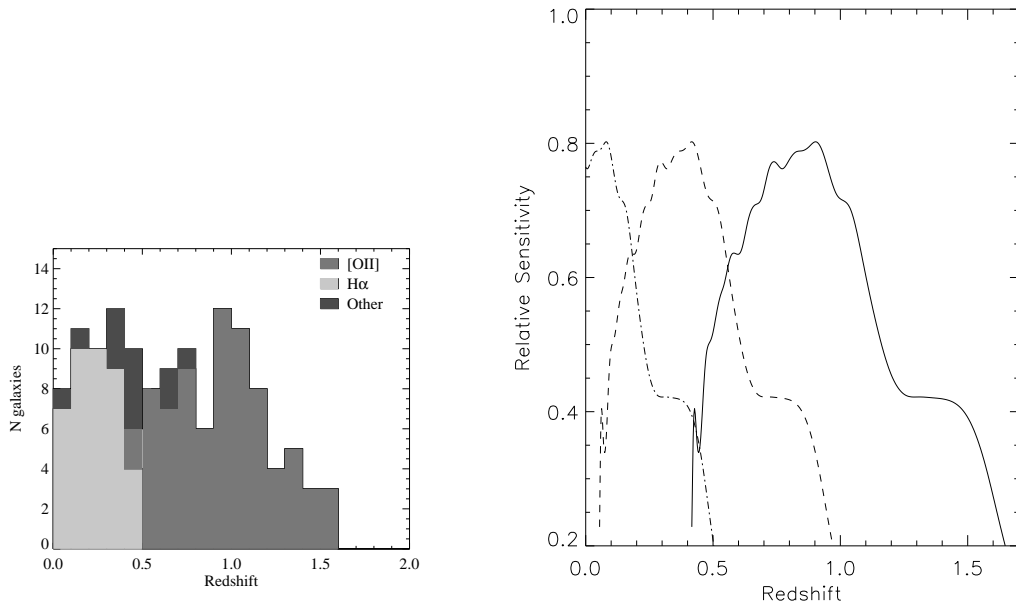


Fig. 25.— a: The distribution of redshifts for emission line objects. The medium grey region indicates the redshift of [OII] emitters, the light grey region that of H $\alpha$  emitters, and the dark grey that objects with neither [OII] nor H $\alpha$ . b: The relative sensitivity of G750L to each emission line as a function of redshift. The solid line indicates they sensitivity to redshift [OII] emission, the dashed line the sensitivity to [OIII]5007 emission, and the dot-dashed line the sensitivity to H $\alpha$  emission.

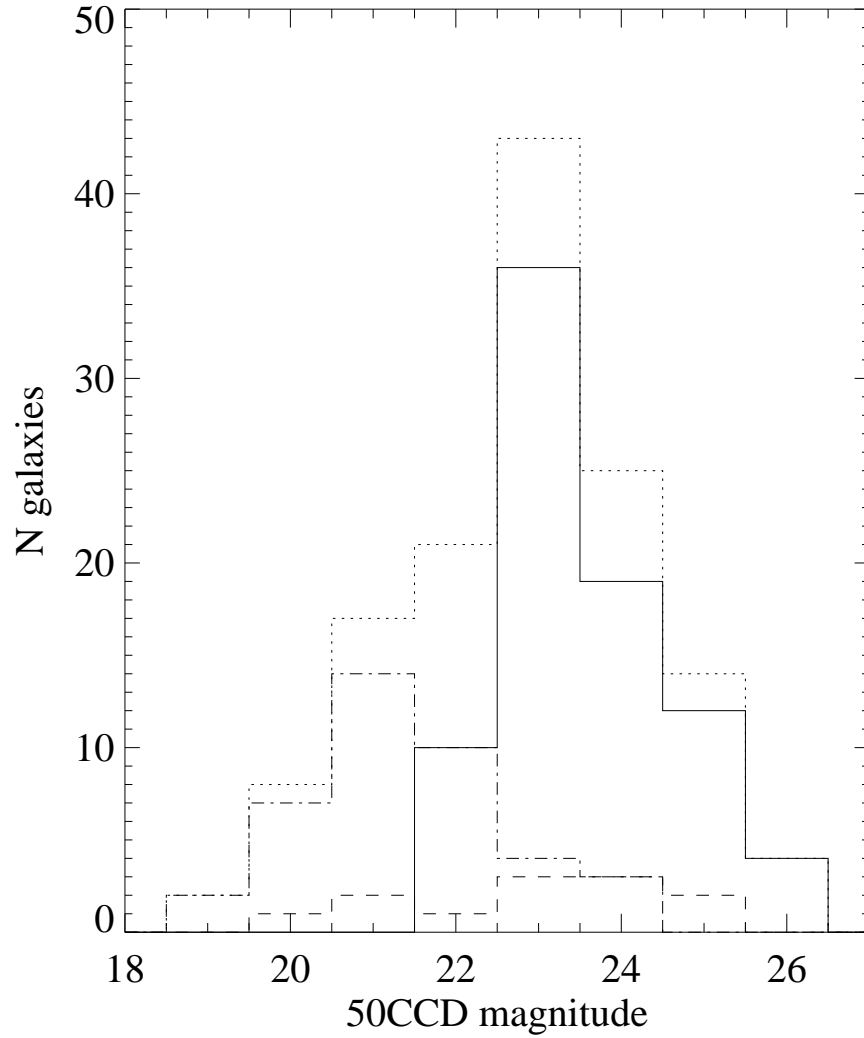


Fig. 26.— The histogram of object photometry for emission line objects. The dotted line shows the histogram for all emission line objects. The solid line indicates the magnitude of [OII] emitters, the dot-dashed line that of H $\alpha$  emitters and the dashed line that objects with neither [OII] nor H $\alpha$ .